



OPEN ACCESS

EDITED BY

Ana Hortência Fonsêca Castro,
Universidade Federal de São João del-Rei, Brazil

REVIEWED BY

Wei-Ting Kuo,
National Taiwan University, Taiwan
Ana De Paula,
Federal Institute of Minas Gerais, Brazil

*CORRESPONDENCE

Yi Wu,
✉ wuyi2001cn@163.com
Adeljiang Wusiman,
✉ adeli5621231@163.com
Qingyong Guo,
✉ dyggy@edu.xjau.cn

RECEIVED 03 May 2024

ACCEPTED 22 July 2024

PUBLISHED 15 August 2024

CITATION

Li J, Yin W, Liang Y, Yang Z, Li L, Mai Z, Yu X, Lu Y, Zhang Z, Abula S, Wu Y, Wusiman A and Guo Q (2024), Pomegranate flower polysaccharide improves mastitis in mice by regulating intestinal flora and restoring the blood-milk barrier.
Front. Pharmacol. 15:1427355.
doi: 10.3389/fphar.2024.1427355

COPYRIGHT

© 2024 Li, Yin, Liang, Yang, Li, Mai, Yu, Lu, Zhang, Abula, Wu, Wusiman and Guo. This is an open-access article distributed under the terms of the [Creative Commons Attribution License \(CC BY\)](https://creativecommons.org/licenses/by/4.0/). The use, distribution or reproduction in other forums is permitted, provided the original author(s) and the copyright owner(s) are credited and that the original publication in this journal is cited, in accordance with accepted academic practice. No use, distribution or reproduction is permitted which does not comply with these terms.

Pomegranate flower polysaccharide improves mastitis in mice by regulating intestinal flora and restoring the blood-milk barrier

Jianlong Li¹, Wen Yin², Yuan Liang¹, Zhaoran Yang¹, Liangliang Li³, Zhanhai Mai¹, Xingjian Yu⁴, Yabin Lu¹, Zhenping Zhang¹, Saifuding Abula¹, Yi Wu^{2,5*}, Adeljiang Wusiman^{1*} and Qingyong Guo^{1*}

¹College of Veterinary Medicine, Xinjiang Agricultural University, Urumqi, China, ²College of Veterinary Medicine, Nanjing Agricultural University, Nanjing, China, ³College of Animal Science and Veterinary Medicine, Henan Agricultural University, Zhengzhou, China, ⁴Department of Biochemistry and Molecular Medicine, School of Medicine, University of California, Davis, CA, United States, ⁵College of Veterinary Medicine, Yunnan Agricultural University, Kunming, China

This study explored the inhibitory effect of pomegranate flower polysaccharide (PFPS) on mastitis through *in vitro* and *in vivo* models. PFPS is a new type of polysaccharide isolated and extracted from pomegranate flowers. The result revealed that PFPS consists of GalA, Ara, and Gal, and the residues consist of 1,4-GalpA, 1,4-Galp, and 1,3,6-Galp, which contain HG-type and RG-I-type pectin structural domains. *In vitro* studies showed that PFPS could inhibit LPS-enhanced phagocytosis of RAW 264.7 cells and the release of IL-1 β , IL-10, and TNF- α . *In vivo*, studies showed that PFPS improved xylene-induced mouse ear swelling and carrageenan-induced mouse paw edema by inhibiting inflammatory factors. In the mouse mastitis model, PFPS significantly improved LPS-induced inflammation and oxidative stress in mammary tissue. Intestinal flora sequencing results showed that PFPS could effectively regulate the intestinal flora of mice, reduce the relative abundance of pathogenic bacteria *Oscillospira* and *AF12*, and increase the probiotics *Blautia*, *Parabacteroides*, *Allobaculum*, and *Clostridiaceae_Clostridium*. Therefore, PFPS ultimately played a role in preventing mastitis by regulating the intestinal flora and further improving the blood-milk barrier. This study provides a scientific basis for PFPS as a potential candidate drug for the treatment of mastitis.

KEYWORDS

Punica granatum, anti-inflammation effect, gut microbiota, RAW 264.7, ear swelling, paw swelling

1 Introduction

Mastitis is a common animal disease in actual production activities, which is manifested by hard, swollen, painful and feverish udders (Sun et al., 2022). Mastitis has a serious impact on animal health and dairy products, specifically: reduced milk production, affected dairy product quality, increased breeding costs, weakened reproductive performance, and threatened public health (Hu et al., 2019). The causes of animal mastitis are complex

and diverse, among which pathogenic microorganisms account for the highest proportion (Gillespie and Oliver, 2005). Currently, the most commonly used and most effective treatment is the use of antibiotics. However, due to the abuse of antibiotics, the number of drug-resistant strains has increased and drug residues have endangered public health (Hu et al., 2019). Therefore, the development of alternative drugs to antibiotics has become a research focus. Neutrophil infiltration in breast tissue is the main diagnostic criterion for mastitis (Guidry et al., 1998). The blood-milk barrier is mainly composed of mammary epithelial cells and tight junctions between cells (Tsugami et al., 2017). The increase in the permeability of the blood-milk barrier promotes the migration of neutrophils, so maintaining the blood-milk barrier is important for inhibiting mastitis (Wang et al., 2017a). Recent studies have reported that intestinal flora plays an important regulatory role in maintaining the blood-milk barrier. For example, the bacterial metabolite Lipopolysaccharide (LPS) increases the permeability of the blood-milk barrier, while short chain fatty acid (SCFA) can restore the blood-milk barrier by increasing the content of tight junction proteins (Wang et al., 2017b). Improving mastitis by regulating intestinal flora and maintaining the blood-milk barrier has become a popular research direction.

Pomegranate (*Punica granatum* L.) belonging to the Lythraceae family, is a cash crop with great economic value cultivated worldwide (Caruso et al., 2020). Although the pomegranate is more commonly regarded as a fruit, the leaves, flowers, pericarp, and roots from pomegranate shrubs have been applied in the treatment of numerous diseases, giving the pomegranate significant value as traditional medicines (Faria and Calhau, 2011; Karimi et al., 2017; Vucic et al., 2019). For example, pomegranate leaf is an important recipe in traditional Chinese medicine for hemostatic purposes, which can be used to relieve nosebleeds, external bleeding, vomiting blood, and other symptoms of the disease (Lansky and Newman, 2007; Colombo et al., 2013); the extract of pomegranate bark is reported as antibacterial agent to treat antibiotic resistant pathogens (Leesombun et al., 2022); the tannins and flavonoids from pomegranate peel show good antihyperglycemic, antihepatoprotective and antioxidant effects (Middha et al., 2013). Other researches have unveiled the therapeutic capabilities of pomegranate such as anti-inflammatory (Xu D. et al., 2022), antioxidant (Wei et al., 2022), anti-diabetic (Li et al., 2008), vasoprotective (Wang et al., 2018), and neuroprotective (George et al., 2023) functions. In general, the medicinal values of pomegranate are still being discovered and developed, and its pharmacological properties can be attributed to the enriched and diverse secondary metabolites, such as ellagic acid, punicalagin, alkaloids, and phenolics (Wibaut and Hollstein, 1957; Liu and Seeram, 2018; Hosseini et al., 2023). However, among numerous publications on *P. granatum*, few have reported the chemical structure and pharmacological activities of polysaccharide from pomegranate flower. Polysaccharides have a significant regulatory effect on the microbiota and can be converted into SCFA by the microbiota to regulate the metabolic process of animals (Aoki et al., 2021). Studies have shown that improving intestinal flora can promote the expression of tissue barrier proteins and ultimately inhibit the occurrence of tissue inflammation (Li et al., 2023; Ran et al., 2024). Ran et al. (2024) used FMT experiments to confirm that Hesperetin improves the blood-milk barrier by

regulating intestinal flora to inhibit the activation of the TLR4/NF- κ B signaling axis, ultimately inhibiting the occurrence of mastitis in mice. Li et al. (2023) found that Maslinic acid can promote the expression of barrier proteins in mammary tissue through intestinal flora, thereby inhibiting mastitis. Therefore, we proposed a scientific hypothesis on whether PFPS can improve the blood-milk barrier by regulating intestinal flora and ultimately inhibit mastitis.

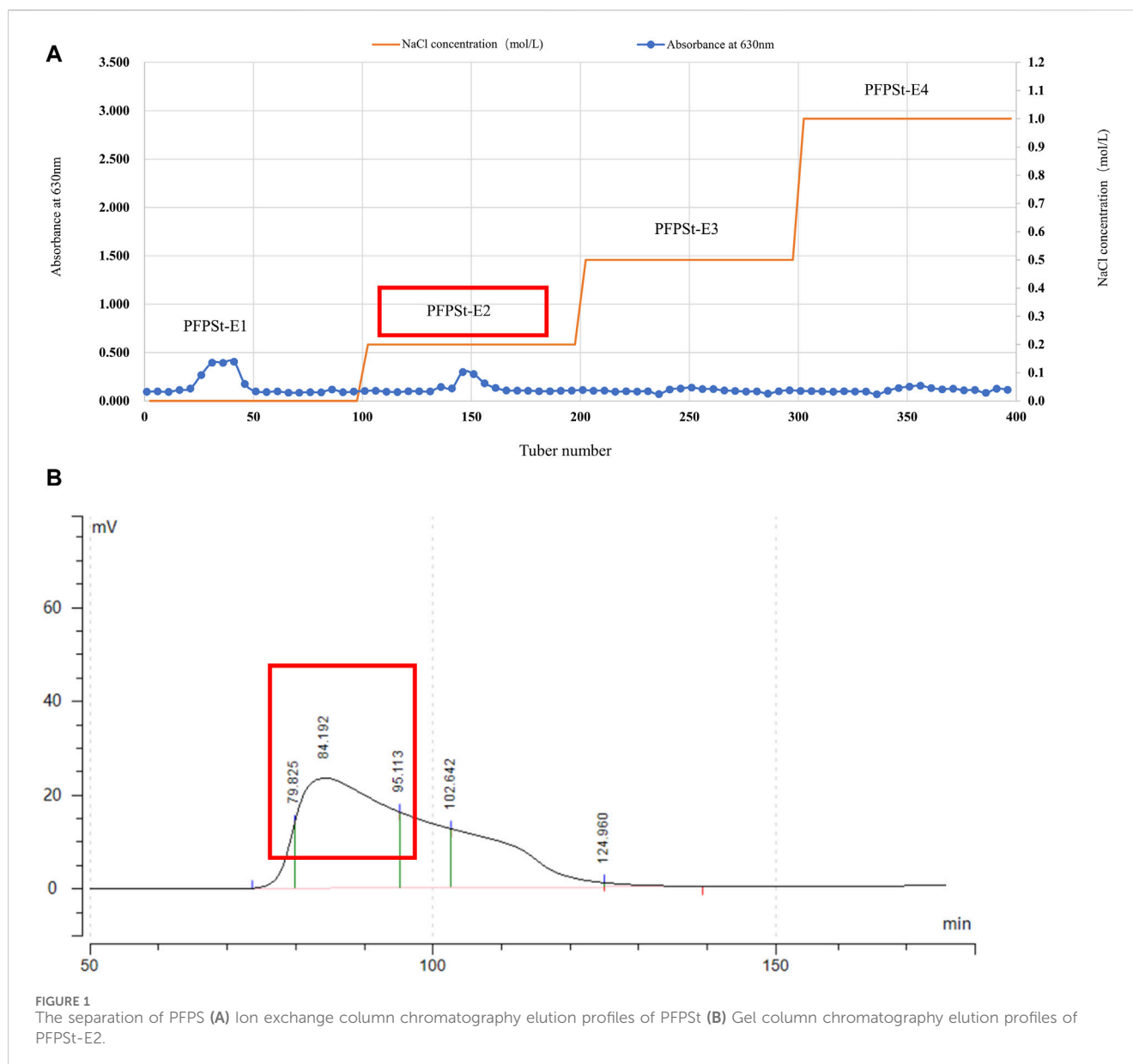
2 Materials and methods

2.1 Materials and reagents

Dulbecco's Modified Eagle Medium (DMEM) was purchased from Thermo Scientific; Dexamethasone (DEX) sodium phosphate injection was purchased from Shanxi Ruicheng Kelong Veterinary Drug Co., Ltd.; Lipopolysaccharide (LPS) was purchased from Sigma-Aldrich; Vybrant phagocytosis assay kit was purchased from Molecular Probes; Trizol reagent and reverse transcription kit were purchased from Life Technologies; TNF- α and IL-6 kit were both purchased from Neobioscience; IL-1 β was purchased from Wuhan Boster Biological Technology, LTD.; CAT, SOD, MDA, GSH, T-AOC and MPO kit were purchased from Nanjing Jiancheng Biological Engineering Research Institute; ZDM-1101 enzyme labeler was purchased from Droide Instrument Equipment Shanghai Co., Ltd.; TGL-16A centrifuge was purchased from Changsha Pingfan Instrument and Meter Co., Ltd.; CO₂ incubator was purchased from Thermo Fisher Scientific Co. Ltd.; TS100 inverted microscope was purchased from Nikon; FACSAria II flow cytometer was purchase from Becton, Dickinson, and Company.

2.2 Separation and purification of PFPS

Pomegranate flower was purchased from the Second People's Hospital of Xinjiang Uygur Autonomous Region and specimen (No. 20200302) was deposited in College of Veterinary Medicine, Xinjiang Agricultural University. The pomegranate flowers (1 kg) were refluxed with 95% ethanol (5 L) at 65°C under reduced pressure twice for 5 h each. Then, add 8 times the amount of pure water and heat for 4 h. The two filtrates were combined and 90% ethanol was added to the filtrate to give a final concentration of 80% to yield the crude PFPSt (total crude polysaccharides of Pomegranate flower) after 24 h. The crude PFPSt was dissolved in pure water and added to sewage reagent five times to remove proteins, followed by spinning under reduced pressure to remove organic reagents. Then the remaining water content was removed by lyophilization. The crude PFPSt (30 g) extract was reconstituted in water (300 mL). The resulting PFPSt solution was centrifuged at 8,000 rpm for 10 min and then filtered through a 0.45 μ m microporous membrane to remove the insoluble precipitates. Then the filtrate was purified by ion-exchange chromatography column (DEAE sepharose FF) and eluted with deionized water of deionized water (dH₂O), 0.2 M NaCl, 0.5 M NaCl, and 1.0 M NaCl successively to collect the eluted



fractions. The sugar content of each eluted fractions was analyzed by the phenol-sulfuric acid method to give the elution peak. The experiment of phenol-sulfuric acid quantitative method was based on the method of [Yue et al. \(2022\)](#). dH₂O and 0.2 M NaCl solution eluted more polysaccharides than 0.5 M NaCl and 1.0 M NaCl solutions. Considering that the molecular weight eluted from 0.2 M NaCl was more compatible, the 0.2 M NaCl elution fraction was selected for purification by gel filtration column chromatography ([Figure 1A](#)). Eluted fractions were performed on a gel filtration chromatography column (Chromdex 200PG), eluted with ultrapure water. Eluted fractions of the peak (80–95 min) were collected, combined, and named PFPS ([Figure 1B](#)). Then the eluate fractions were concentrated under reduced pressure and freeze-dried under a vacuum. The ion-exchange chromatography column and gel filtration column chromatography were performed using the method we reported previously ([Wu et al., 2022](#)).

2.3 Characterization of the PFPS

2.3.1 Molecular weight of PFPS

The dextran standards (1, 5, 12, 25, 50, 80, 150, 270, 410, and 670 kDa) was diluted by 0.05 M NaCl solution to make 5 mg/mL dextran standard solutions. The molecular weight of PFPS was performed by High-Performance Gel Permeation Chromatography ([Yang et al., 2023](#)). The standard solution was added to PFPS to formulate test sample solutions with 5 mg/mL PFPS.

2.3.2 Monosaccharide composition of PFPS

1 mL of 2 M trifluoroacetic acid solution was added to 5 ± 0.1 mg PFPS sample and the mixture was heated at 121°C for 2 h. Then the extracts were concentrated by centrifugation, reconstituted with sterile water, and analyzed by chromatography to determine the monosaccharide composition of PFPS. Using Chromeleon, the

content of each component in the sample ($\mu\text{g}/\text{mg}$) was calculated according to the formula = $C \times V \times F/M$ (C is the instrumental reading concentration, V is the volume of sample extract, F is the dilution factor, and M is the total amount of sample weighed).

2.3.3 Elucidation of PFPS linkage

PFPS (10 mg) extract was dissolved in ultrapure water (1 mL), followed by addition of 100 mg/mL carbodiimide (1 mL). After 2-h incubation, the solution was divided into two groups and 2 M imidazole (1 mL) was added separately. 1 mL of 30 mg/mL of NaBH_4 and 1 mL of 30 mg/mL of NaBD_4 were added to each solution and the mixture was incubated for 3 h. The reaction was terminated by the addition of 100 μL of glacial acetic acid to obtain the reduced sample. The samples were dialyzed for 48 h and lyophilized. The lyophilized PFPS was dissolved in 500 μL DMSO, and 1 mg NaOH was added and incubated for 30 min. Then 50 μL of iodomethane solution (30 mg/mL) was added to methylated all hydroxyl groups, followed by 1 mL water and 2 mL dichloromethane were added, which were further centrifuged to obtain the dichloromethane phase. Subsequently, the PFPS was hydrolyzed to monosaccharides to further determine the linkage of the sugar residues. Firstly, 100 μL of 2 M TFA was added, and the reaction was carried out at 121°C for 90 min. Then, 50 μL of 2 M ammonia and 50 μL of 1 M NaBD_4 were added, which was carried out at room temperature for 2.5 h. The reaction was terminated by the addition of 20 μL of acetic acid, followed by the addition of 250 μL of acetic anhydride, which was carried out at 100°C for 2.5 h. Finally, 1 mL water and 500 μL methylene chloride were added, and the dichloromethane phase was taken for detection after centrifugation.

2.3.4 Nuclear magnetic resonance (NMR) analysis of PFPS

The lyophilized samples were dissolved in 0.5 mL D_2O and TMSP was added as an internal standard. One-dimensional (^1H -NMR and ^{13}C -NMR) and two-dimensional (including ^1H - ^1H COSY, TOCSY, HSQC, HMBC, and NOESY) were determined using a 600 MHz Bruker NMR spectrometer.

2.4 In vitro anti-inflammatory activity of PFPS

2.4.1 Cell viability

RAW264.7 cells were purchased from American Type Culture Collection (ATCC). RAW 264.7 cells in the logarithmic growth phase were adjusted to 5×10^5 cells/mL, cultured in 96-well plates at 100 μL per well, and placed in a 37°C , 5% CO_2 incubator for 24 h. After discarding the culture medium in the wells, 100 μL of different concentrations of PFPS (1,000, 500, 250, 125, and 62.5 $\mu\text{g}/\text{mL}$) made from DMEM cell culture medium were added to each well with explicated experiments for each concentration. After 24 h of incubation, CCK-8 solution was used to evaluate the cell viability.

2.4.2 Inflammatory factor

RAW 264.7 cells in PFPS-treated groups were cotreated with different concentrations of PFPS (62.5, 125, 250 $\mu\text{g}/\text{mL}$) and LPS (1 $\mu\text{g}/\text{mL}$) for 24 h. The Model group only used LPS (1 $\mu\text{g}/\text{mL}$)

TABLE 1 Primers for qRT-PCR.

Symbol	Primer sequences (5'-3')
Mouse-TNF- α	Forward: CACCACGCTCTTCTGTCTACTGAAC
	Reverse: AGATGATCTGAGTGTGAGGGTCTGG
Mouse-IL-6	Forward: ACTTCCAGCCAGTTGCCTTCTTG
	Reverse: TGGTCTGTTGTGGGTGGTATCCCTC
Mouse-IL-1 β	Forward: CACTACAGGCTCCGAGATGAACAAC
	Reverse: TGTCGTTGCTTGGTTCTCCTTGTAC
Mouse-GPX3	Forward: AACGTAGCCAGCTACTGAGGTCTGA
	Reverse: CCACCTGGTCCGAACATACTTGAGAC
Mouse-GPX1	Forward: TTCCCTCAAGTACGTCGCACCTG
	Reverse: TCTCACCATTCACTTCGCACTTCTC
Mouse-SOD2	Forward: TCCCAGACCTGCCTTACGACTATG
	Reverse: CTCCTCGGTGGCGTTGAGATTG
Mouse-CAT	Forward: CCATAGCCAGAAGAGAAACCCACAG
	Reverse: GGAATCCCTCGGTCACTGAACAAG
Mouse-Occludin	Forward: ACGGACCCTGACCACTATGA
	Reverse: TCAGCAGCAGCCATGTACTC
Mouse-Claudin-3	Forward: CCACCATTGGCATGAAGTGC
	Reverse: AGAGGTTGTTTTCCGGGGAC
Mouse-Actb	Forward: GTGACGTTGACATCCGTAAGA
	Reverse: GCCGGACTCATCGTACTCC

modeling. The supernatant was collected to determine the content of IL-1 β , TNF- α , and IL-10 by ELISA kits.

2.4.3 Phagocytic ability of neutral red

The cell processing method is the same as 2.4.2. After incubation for 24 h, add 100 μL of 0.1% neutral red to each well and continue incubation for 1 h. Rinse twice with PBS to remove excess neutral red, and finally add 100 μL cell lysate (ethanol and 0.01% acetic acid at the ratio of 1:1) to each well. After incubation at 4°C overnight, the samples were measured at the absorbance of 540 nm by a microplate reader.

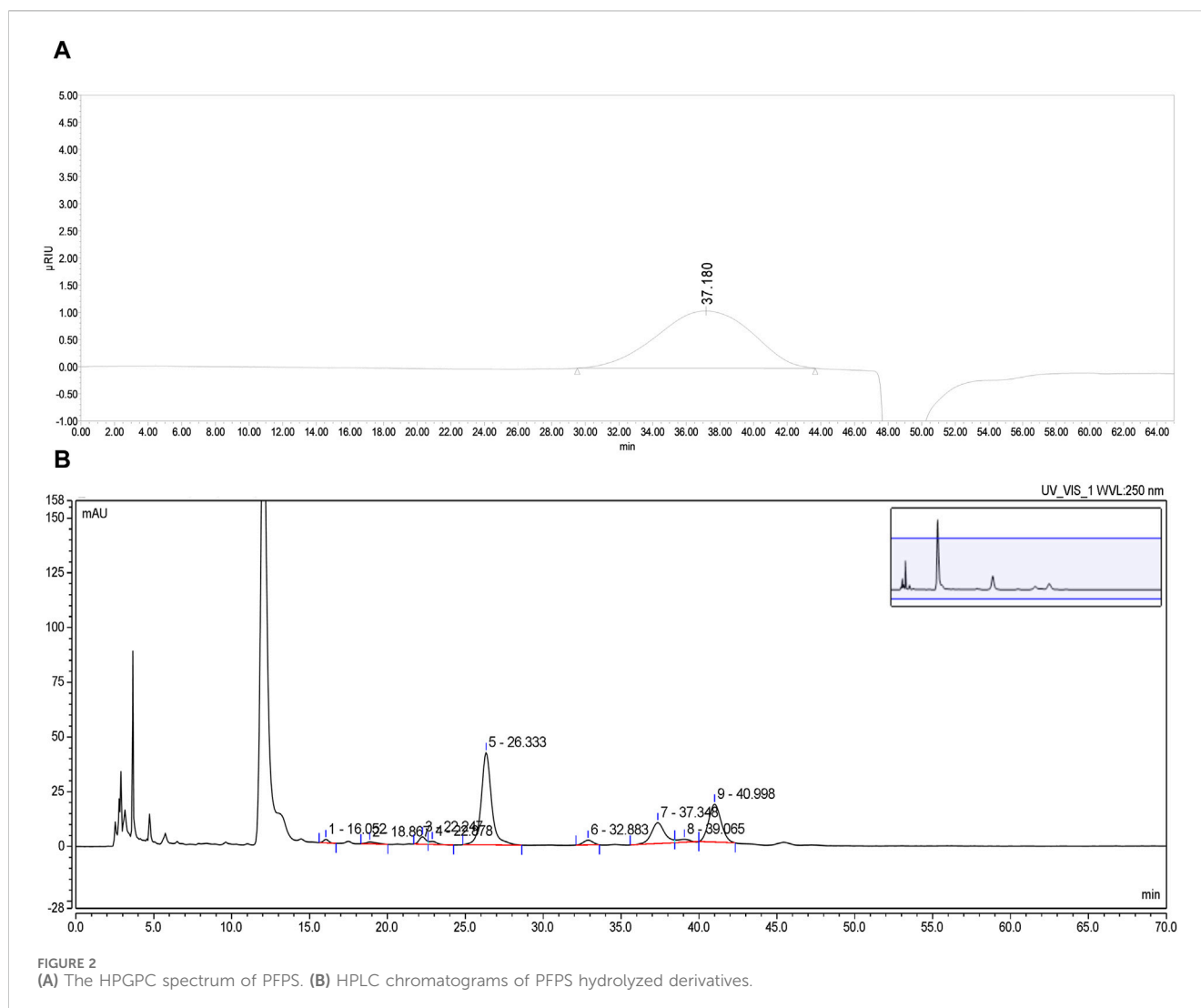
2.4.4 Phagocytic ability of *Escherichia coli*

The cell processing method was consistent with 2.4.2. After incubation for 24 h, the FITC-labeled *Escherichia coli* solution supplied by Vybrant phagocytosis assay kit was added to the cells and incubated for 2 h. Finally, 100 μL of Taipan blue suspension was added and the phagocytosis rate was determined by flow cytometry.

2.5 In vivo anti-inflammatory activity of PFPS

2.5.1 Animals

All mice were purchased from Liaoning Changsheng Biotechnology Co., Ltd. and kept at the Laboratory Animal Center of Xinjiang Agricultural University with a standard diet



and in standard specific pathogen-free (SPF) conditions between 20°C and 23°C, with 12 h light/dark cycles. Animal experiments were performed in compliance with the guidelines of the Xinjiang Agricultural University Institutional Animal Care and Use Committee (IACUC), detailed in the IACUC-approved protocol (No. 2022009). All animals were adaptively reared for 1 week before the formal experiment.

2.5.2 Mouse ear Edema's swelling test

Thirty-six Kunming mice (half females and half males, 6–8 weeks) were divided into six groups randomly: Control group, Model group, DEX group, PFPS-L group, PFPS-M group, and PFPS-H group. The Control group and Model group were gavaged with saline. The DEX group was gavaged with dexamethasone (10 mg/kg). The PFPS groups were gavaged with diverse doses of PFPS (PFPS-L: 400 mg/kg; PFPS-M: 800 mg/kg; PFPS-H: 1,600 mg/kg, 20 mL/kg). Each group was treated for 7 days. 1 h after the last administration on day 7, dimethylbenzene (0.03 mL) was smeared on both sides of the right ear of each mouse in the Model group, DEX group, and PFPS-treated groups, while mice of the Control group were treated with saline

(0.03 mL) as the same method. 0.5 h after administration of the dimethylbenzene/saline, the peripheral blood of each mouse was harvested from the heart. Then the mouse was sacrificed by cervical dislocation and the whole ears of each mouse (both treated and untreated) were collected and stacked symmetrically, and then a hole puncher (8 mm in diameter) was used to collect the ear fractions. The weight of each ear fraction was tested to calculate the inhibition ratio, the swelling rate and inhibition rate were calculated as follows.

$$\text{Swelling Rate \%} = \frac{\text{Weight of Right ear fraction} - \text{Weight of left ear fraction}}{\text{Weight of left ear fraction}} \times 100\%$$

$$\text{Inhibition rate \%}$$

$$= \frac{\text{Average swelling rate of inflammation group} - \text{Average Swelling rate of administration group}}{\text{Average swelling rate of inflammation group}} \times 100\%$$

2.5.3 Carrageenan-induced paw edema assay

Thirty-six Kunming mice (half females and half males, 6–8 weeks) were divided into six groups randomly: Control group, Model group, DEX group, PFPS-L group, PFPS-M group, and PFPS-H group. The Control group and Model group were

TABLE 2 The molecular weight and physicochemical chemical composition of PFPS.

Sample PFPS	
Mp (kDa)	29.139
Mw (kDa)	36.250
Mn (kDa)	24.285
Monosaccharide compositions (%)	
Galacturonic Acid (GalA)	56.735
Arabinose (Ara)	20.631
Galactose (Gal)	12.020
Rhamnose (Rha)	5.267
Glucose (Glc)	1.550
Glucuronic Acid (GlcA)	1.341
D-Glucosamine hydrochloride (GlcN)	1.020

gavaged with saline. The DEX group was gavaged with dexamethasone (10 mg/kg). The PFPS groups were gavaged with diverse doses of PFPS (PFPS-L: 400 mg/kg; PFPS-M: 800 mg/kg; PFPS-H: 1,600 mg/kg, 20 mL/kg). Each group was treated for 7 days. 1 h after the last administration on day 7, 1% carrageenan (50 μ L) was injected into the voix pedis of the right-hind limb of each mouse in DEX, Model, and PFPS-treated groups, and the mouse in the control group was treated with saline following the same method. At the time points of 0, 1, 2, 3, 4, 5, 6, and 7 h after the injection, the thickness of the right-hind limb for each mouse was measured three times and the swelling ratio and inhibition ratio were calculated as follow.

Swelling Rate % =

$$\frac{\text{Thickness of Voix Pedis after injection} - \text{Thickness of Voix Pedis before injection}}{\text{Thickness of Voix Pedis after injection}} \times 100\%$$

2.5.4 Construction of the mouse mastitis model

Seventy-two Kunming mice (42 females and 21 males) were divided into six groups: Control group, Model group, DEX group (5 mg/kg dexamethasone), PFPS-L group (400 mg/kg PFPS), PFPS-M group (800 mg/kg PFPS), PFPS-H group (1,600 mg/kg PFPS). Pregnant female mice were separated after 1 week of combined cage rearing. After the females gave birth, the females were separated from the pups, when the body color of the pups changed from dark red to slightly reddish. The Control and Model groups were gavaged with saline from day 7 to day 14, and the Control group used PBS modeling on day 15. The DEX group was gavaged with dexamethasone from day 7 to day 14. The PFPS groups were given diverse doses of PFPS from day 7 to day 14. On day 15, mastitis models were established in all groups except the Control group. To establish a mouse mastitis model, 0.3% sodium pentobarbital solution was injected intraperitoneally for anesthesia, 1 mm of the nipple was cut off with ophthalmic scissors to expose the milk ducts, and 50 μ L of 0.2 mg/mL LPS solution was slowly injected into the mammary gland.

2.5.5 Inflammatory factor and oxidative stress markers

The content of IL-1 β , TNF- α , IL-10, CAT, SOD, MPO, GSH, MDA, and T-AOC in tissue was determined following the kit manual Section 2.4.2.

2.5.6 HE staining and immunofluorescence

The ear and breast tissues of mice were fixed with 10% neutral formalin solution and submitted to Powerful Biology Co., Ltd. (Wuhan, China) for staining. The quantification was performed by ImageJ.

2.5.7 16S rRNA sequencing analysis

Fresh colon stool samples frozen in liquid nitrogen were submitted to Personalbio Biotechnology Co., Ltd. (Shanghai, China) for 16S rRNA sequencing analysis. Experimental results are uploaded to the GenesCloud Platform for data analysis.

2.5.8 qPCR

Trizol was used for RNA extraction reagent followed by reverse transcription into cDNA using the provided kit as per the manufacturer's instructions. SYBR Green PCR Master Mix was employed for conducting qPCR following the instructions provided by the manufacturer. The primer sequences used are listed in Table 1.

2.6 Statistical analysis

All results are expressed as the mean \pm standard deviation, graphed by GraphPad Prism 6.0 software for ANOVA multiple comparisons. $P < 0.05$ is considered statistically significant in this analysis.

3 Result

3.1 The characterization of PFPS

PFPS is a polysaccharide extracted and purified from Pomegranate flowers. The HPGPC detection result showed a single symmetrical peak (37.18 min), so PFPS was a purified polysaccharide with a single composition (Figure 2A). By comparing the chromatograms with those of 11 monosaccharide standards, it was determined that PFPS was mainly composed of Galacturonic Acid, Arabinose, Galactose and Rhamnose (Figure 2B). The molecular weight and physicochemical chemical composition of PFPS summarized in Table 2.

The results of the methylation analysis mainly contained 1,4-GalpA sugar residues and contained 1,4-Galp, 1,3,6-Galp, t-Araf, 1,5-Araf, 1,2,5-Araf, and 1,2,4-Rhap sugar residues, suggesting that the polysaccharide samples may contain HG-type and RG-I-type pectin structural domains. The detailed connection mode was shown in Table 3.

The ¹H-NMR spectrum (Figure 3A) showed proton resonance signals concentrated in the region of δ 3.0–5.5 ppm and δ 4.5–5.5 ppm, suggesting the presence of a variety of sugar residues. ¹³C-NMR spectrum (Figure 3B) showed the presence of reduced telomeric end-groups at δ 93.52 ppm and δ 97.39 ppm, which were presumed to belong to the C-1 signal peaks of the

TABLE 3 The sugar residue connection mode of PFPS.

Connection type	Derivative name	RT	Molar ratio
T-Araf	1,4-di-O-acetyl-2,3,5-tri-O-methyl arabinitol	11.686	3.466
T-Rhap	1,5-di-O-acetyl-6-deoxy-2,3,4-tri-O-methyl rhamnitol	12.708	1.641
1,3-Araf	1,3,4-tri-O-acetyl-2,5-di-O-methyl arabinitol	14.500	0.824
1,5-Araf	1,4,5-tri-O-acetyl-2,3-di-O-methyl arabinitol	15.425	4.618
T-GalpA	1,5-di-O-acetyl-2,3,4,6-tetra-O-methyl galactitol	17.449	5.763
1,3,5-Araf	1,3,4,5-tetra-O-acetyl-2-O-methyl arabinitol	17.954	1.774
1,2,4-Rhap	1,2,4,5-tetra-O-acetyl-6-deoxy-3-O-methyl rhamnitol	18.381	1.481
1,4-GalpA	1,4,5-tri-O-acetyl-2,3,6-tri-O-methyl galactitol	19.849	68.706
1,4-Galp	1,4,5-tri-O-acetyl-2,3,6-tri-O-methyl galactitol	19.849	2.255
1,2,3,5-Araf	1,2,3,4,5-penta-O-acetyl arabinitol	20.011	1.548
1,3-Galp	1,3,5-tri-O-acetyl-2,4,6-tri-O-methyl galactitol	20.308	1.286
1,6-Galp	1,5,6-tri-O-acetyl-2,3,4-tri-O-methyl galactitol	21.538	0.923
1,3,4-GalpA	1,3,4,5-tetra-O-acetyl-2,6-di-O-methyl galactitol	21.952	0.844
1,2,4-GlcpA	1,2,4,5-tetra-O-acetyl-3,6-di-O-methyl glucitol	22.547	0.718
1,4,6-GalpA	1,4,5,6-tetra-O-acetyl-2,3-di-O-methyl galactitol	23.517	0.708
1,3,6-Galp	1,3,5,6-tetra-O-acetyl-2,4-di-O-methyl galactitol	24.371	3.445

reduced telomeric end-groups α -GalpA (R_{α}) and β -GalpA (R_{β}), respectively. The ^{13}C -NMR spectrum showed a significant inverted signal in the region of δ 60–70 ppm, suggesting the presence of a variety of sugar residues. The DEPT-135 spectrum (Figure 3C) revealed the presence of inverted signals in the region of δ 60–70 ppm, indicating that the sugar residues contain -CH₂- groups.

The resonance signals in the region of δ 1.10–1.27 ppm revealed the presence of methyl protons H-6 of rhamnose (Rha) residues. δ 1.90–2.08 ppm showed the methyl proton signals of the O-acetyl group, and δ 21.25 ppm showed the methyl signals of the acetyl group. The signal at δ 176.44 ppm represented the characteristic absorption peak at the C-6 position in the unesterified galacturonic acid residue, and the corresponding characteristic absorption peak at δ 53.99 ppm represented the characteristic absorption peak at the C-6 position in the esterified galacturonic acid residue. The peak at δ 53.99 ppm represents the methyl carbon attached to the C-6 position in the methylated galacturonic acid residue (Figure 3D). The δ 98–102 ppm signal is presumed to be the hetero-capsule carbon of α -GalpA, and the δ 106–110 ppm is presumed to be the hetero-capsule carbon of the sugar residue α -Araf. The hetero-head signals δ 4.94 ppm (H-1) and δ 100.15 ppm (C-1) of the GA_{1,4} sugar residue were determined as α -configuration from the HSQC and 1H-1H COSY (Figure 3E). 1H-1H COSY showed the signals of H-2, H-3, and H-4, attributed to δ 3.60, δ 3.86, and δ 4.27 ppm, respectively. The chemical shifts of C-1 to C-4 on the sugar ring were determined to be δ 100.15, δ 69.23, δ 69.87, and δ 79.03 ppm, respectively. The chemical shift of C-6 was found to be δ 176.44 ppm in the HMBC spectrum (Figure 3F), which is the characteristic absorption peak in unesterified galacturonic acid residues. Combined with the results of methylation analysis and literature

reports (Figures 3A–G), the GA_{1,4} sugar residue was inferred to be \rightarrow 4)- α -D-GalpA-(1 \rightarrow). The hetero-head signals δ 4.77 ppm (H-1) and δ 101.44 ppm (C-1) were found based on HSQC and 1H-1H COSY, indicating that the $^6\text{MeGA}_{1,4}$ is in the α -configuration. Concerning the results of the monosaccharide composition test and methylation analysis, the residue was hypothesized to be an α -GalpA sugar residue. The H-1, H-2, H-3, and H-4 signals were attributed to δ 4.77, δ 3.59, δ 3.86, and δ 4.33 ppm, respectively. The chemical shifts of C-1~C-4 on the sugar ring as δ 101.44, δ 69.03, δ 69.87, and δ 80.02 ppm, respectively. The existence of a correlation cross-peak between C-6 and methyl proton signals of methyl ester δ 3.67 ppm δ 3.67/172.09 ppm, indicating methylation of the sugar residue. The presence of a correlation cross peak δ 3.67/172.09 ppm between C-6 and methyl proton signals of methyl ester indicated that there was methylation of the sugar residue. The chemical shifts of C-1 and C-4 were shifted towards the lower field, indicating the substitution of the residue at the C-1 and C-4 positions of the sugar ring. Combining the methylation results and literature reports, the $^6\text{MeGA}_{1,4}$ sugar residue was deduced to be \rightarrow 4)- α -GalpA-6-OMe-(1 \rightarrow). Following a similar approach, the major sugar residues H and C chemical shifts were summarized in Table 4. Combining the above results, the backbone chains of the PFPS were deduced as HG-type and RG-I-type pectin structural domains as well as side chains of R1 and R2 (Figure 3H).

3.2 PFPS inhibited LPS-induced activation of RAW264.7 cells

Our study preliminarily evaluated the anti-inflammatory efficacy of PFPS on LPS-induced RAW264.7 cells. As shown in

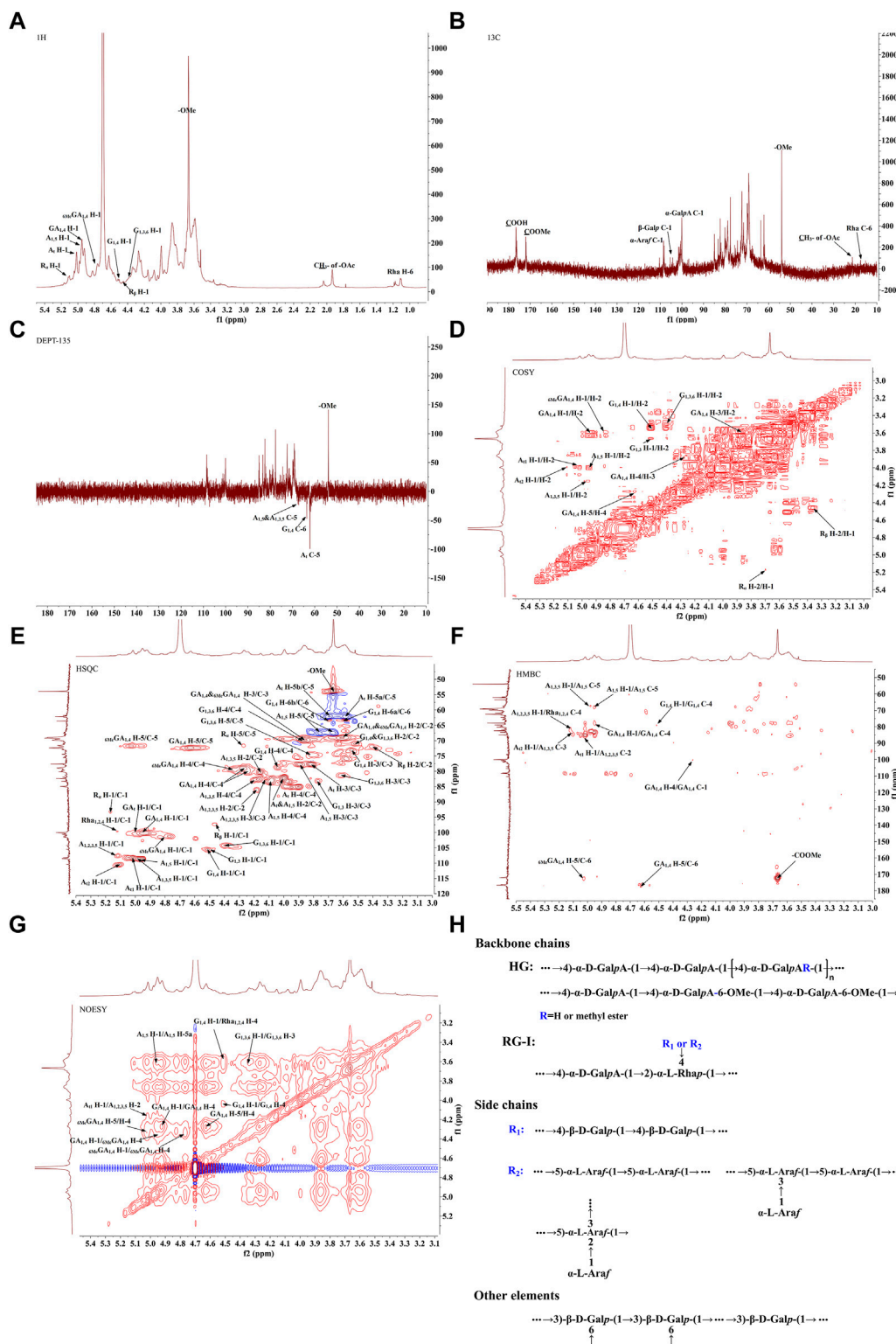


FIGURE 3 The NMR analysis of PFPS. (A) ¹H NMR spectra of PFPS. (B) ¹³C NMR spectra of PFPS. (C) DEPT-135 spectra of PFPS. (D) COSY spectra of PFPS. (E) HSQC spectra of PFPS. (F) HMBP spectra of PFPS. (G) NOESY spectra of PFPS. (H) The structure of PFPS.

Figure 4A, RAW264.7 cell viability decreased under PFPS treatment at doses higher than 250 μg/mL. Therefore, 62.5, 125, and 250 μg/mL PFPS were selected for following experiments, and the corresponding treatment groups were named PSPF-L, PFPS-M, and PFPS-H

respectively. Compared with the Model group, PFPS inhibited the release of IL-1β, IL-6, and TNF-α from LPS-induced RAW264.7 cells (Figures 4B–D). As shown in Figures 4E, F, the phagocytosis of *E. coli* by cells in the Model group was significantly increased, while PFPS

TABLE 4 Chemical shift assignment of ¹H and ¹³C of each sugar residue.

Sugar residues		δ (ppm)							
			1	2	3	4	5a/5b	6a/6b	-OMe
GA _{1,4}	→4)-α-D-GalpA-(1→	H	4.94	3.60	3.86	4.27	4.63		
		C	100.15	69.23	69.87	79.03	72.38	176.44	
⁶ MeGA _{1,4}	→4)-α-D-GalpA-6-OMe-(1→	H	4.77	3.59	3.86	4.33	5.03/4.96		3.67
		C	101.44	69.03	69.87	80.02	71.63	172.09	53.99
GA _t	α-D-GalpA-(1→	H	4.99	3.61	3.87	4.13	4.71		
		C	100.54	69.34	69.66	71.85	72.42	176.32	
G _{1,4}	→4)-β-D-Galp-(1→	H	4.51	3.52	3.54	4.04	3.64	3.59/3.69	
		C	105.59	71.08	73.05	78.74	74.41	63.57	
G _{1,3,6}	→3,6)-β-D-Galp-(1→	H	4.39	3.51	3.61	3.85	3.81	3.79/3.93	
		C	104.27	70.84	81.28	70.14	74.56	69.57	
G _{1,3}	→3)-β-D-Galp-(1→	H	4.50	3.65	3.77	—	—	—	
		C	105.44	71.19	83.06	—	—	—	
A _{1,5}	→5)-α-L-Araf-(1→	H	4.95	3.99	3.89	4.08	3.67/3.75		
		C	108.51	82.32	77.81	83.34	67.60		
A _{1,3,5}	→3,5)-α-L-Araf-(1→	H	4.97	4.16	3.96	4.18	3.70/3.82		
		C	108.56	80.35	83.49	82.71	67.36		
A _{t1}	α-L-Araf-(1→	H	5.02	3.99	3.82	3.90	3.58/3.69		
		C	108.21	82.32	77.71	85.07	62.15		
A _{t2}	α-L-Araf-(1→	H	5.11	3.99	3.82	3.90	3.58/3.69		
		C	110.47	82.32	77.71	85.07	62.15		
A _{1,2,3,5}	→2,3,5)-α-L-Araf-(1→	H	5.12	4.18	4.12	4.18	3.70/3.82		
		C	107.57	86.10	82.38	82.46	67.36		
Rha _{1,2,4}	→2,4)-α-L-Rhap-(1→	H	5.12	4.00	3.92	3.57	3.81	1.12	
		C	99.34	77.41	70.84	81.59	71.63	17.65	
R _α	→4)-α-D-GalpA	H	5.16	3.69	3.83	4.43	4.27	--	
		C	93.52	69.26	69.87	79.94	71.48	--	
R _β	→4)-β-D-GalpA	H	4.47	3.37	3.63	4.24	--	--	
		C	97.39	72.66	73.86	80.09	--	--	

intervention significantly reduced phagocytosis of RAW264.7 cells. And PFPS reduced LPS-induced neutral red uptake (Figure 4G). Therefore, PFPS significantly inhibited the phagocytosis activity in LPS-induced RAW264.7 cells. In summary, our results show that PFPS can significantly improve LPS-induced inflammation in RAW264.7 cells.

3.3 PFPS suppressed inflammation in mouse ear edema and mouse paw edema models

This study used a xylene-induced mouse ear swelling model to evaluate the *in vivo* anti-inflammatory efficacy of PFPS. The results of pomegranate flower polysaccharide on xylene-induced auricle

swelling in mice are shown in Table 5. Compared with the Control group, the swelling degree of the Model group increased significantly, indicating that the modeling was successful. Compared with the model group, both the PFPS-treated groups and the DEX group significantly reduced the swelling of the auricles induced by xylene inflammation. The PFPS-H group had the best anti-inflammatory effect, which was similar to that of the DEX group. The results of the ear tissue pathological sections are shown in Figure 5A. The Model mouse ears exhibited edema, the gaps between collagen fibers increased, and inflammatory cells infiltrated, accompanied by congestion, hemorrhage, and necrosis of tissue cells. Compared with the Model group, the inflammatory cells in the DEX group were significantly reduced but accompanied by edema,

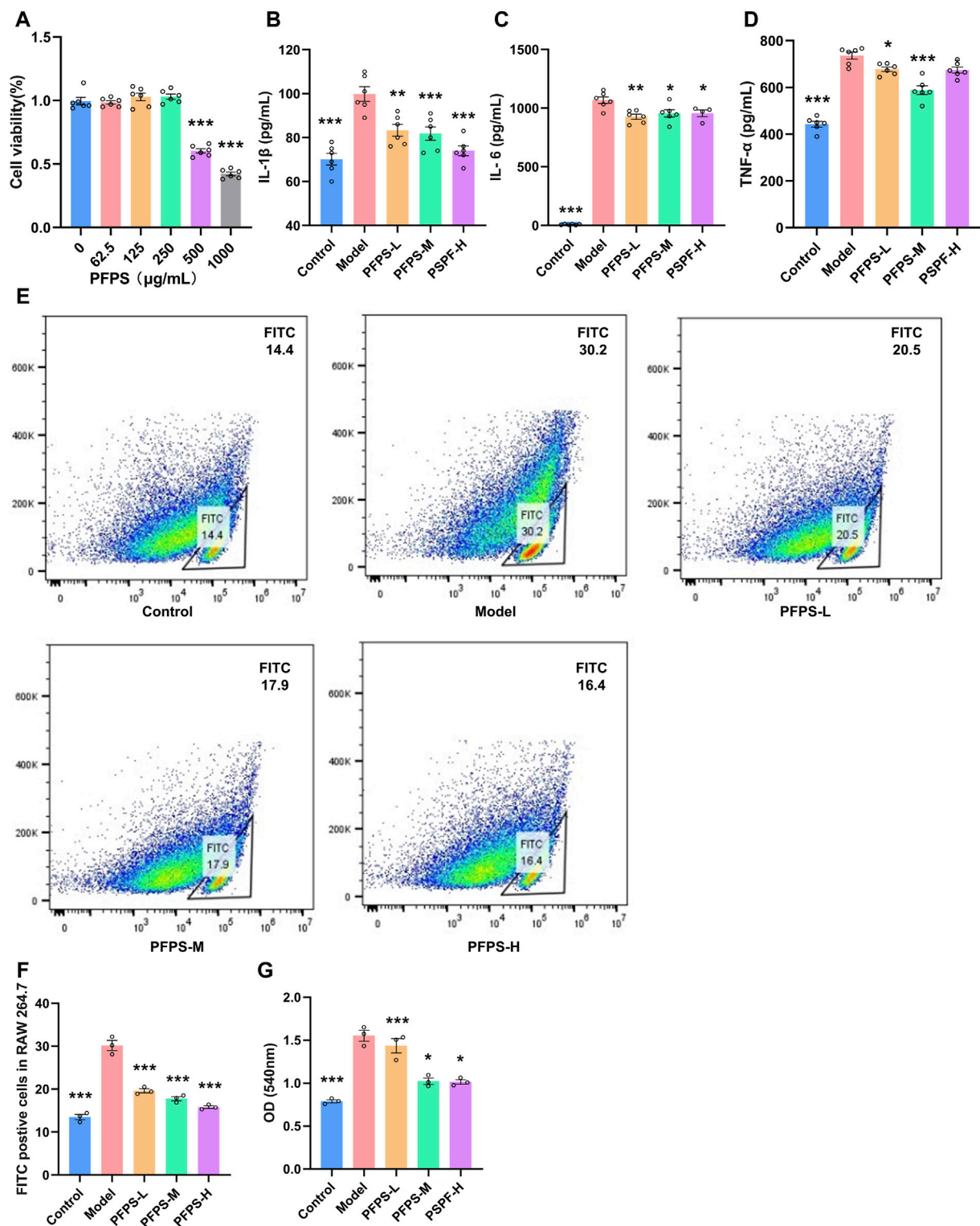


FIGURE 4 PFPS improved inflammation in LPS-induced RAW264.7 cells. **(A)** Cell activity detecting results of RAW264.7 cells treated with PFPS, $n = 6$. **(B–D)** The content of IL-1 β **(B)**, IL-6 **(C)**, and TNF- α **(D)** in all groups, $n = 6$. **(E, F)** Phagocytosis of *Escherichia coli* by RAW 264.7 cells, *Escherichia coli* was marked by FITC, $n = 3$. **(G)** Phagocytosis of neutral red by RAW264.7 cells, $n = 3$. The data represent the means \pm SEM. *: $p < 0.05$, **: $p < 0.01$, ***: $p < 0.001$, vs. Model group.

TABLE 5 Determination of ear edema degree of mice in each group.

Group	Dosage	Inhibition rate (%)	Swelling rate (%)
Control	saline	—	0.001433 ± 0.00132***
Model	saline	—	0.012816 ± 0.00216
PFPS-L	400 mg/kg	15.0033	0.010894 ± 0.00193*
PFPS-M	800 mg/kg	26.5930	0.009408 ± 0.00143**
PFPS-H	1,600 mg/kg	41.8076	0.007458 ± 0.00184**
DEX	10 mg/kg	43.9532	0.007183 ± 0.00117**

Note: *: $p < 0.05$, **: $p < 0.01$, ***: $p < 0.001$, vs. Model group.

congestion, and hemorrhage. In the PFPS supplement group, as the dose increased, related symptoms continued to decrease. In all groups, the PFPS-H group had the best effect, with the fewest inflammatory cells and the least congestion. Consistent with *in vitro* experiments, the level of IL-1 β , IL-6, and TNF- α in ear

tissue were also significantly downregulated affected by PFPS (Figures 5B–D). Therefore, PFPS reduced xylene-induced ear swelling in mice by improving cytokine secretion. Further, our experiments tested the inhibitory effect of PFPS on mouse foot swelling. As the Table 6 showed that different doses of PFPS had a certain inhibitory effect on foot swelling, and the PFPS-H group had the best anti-inflammatory effect. The results of *in vivo* and *in vitro* experiments show that PFPS has significant anti-inflammatory effects.

3.4 PFPS improved LPS-induced mastitis in mice

Our study evaluated the *in vivo* anti-inflammatory effects of PFPS using an LPS-induced mouse mastitis model. As shown in Figure 6, PFPS dose-dependently improved mastitis in mice. Compared with the Control group, the Model group had disordered alveolar structure, widened breast lobule interstitium,

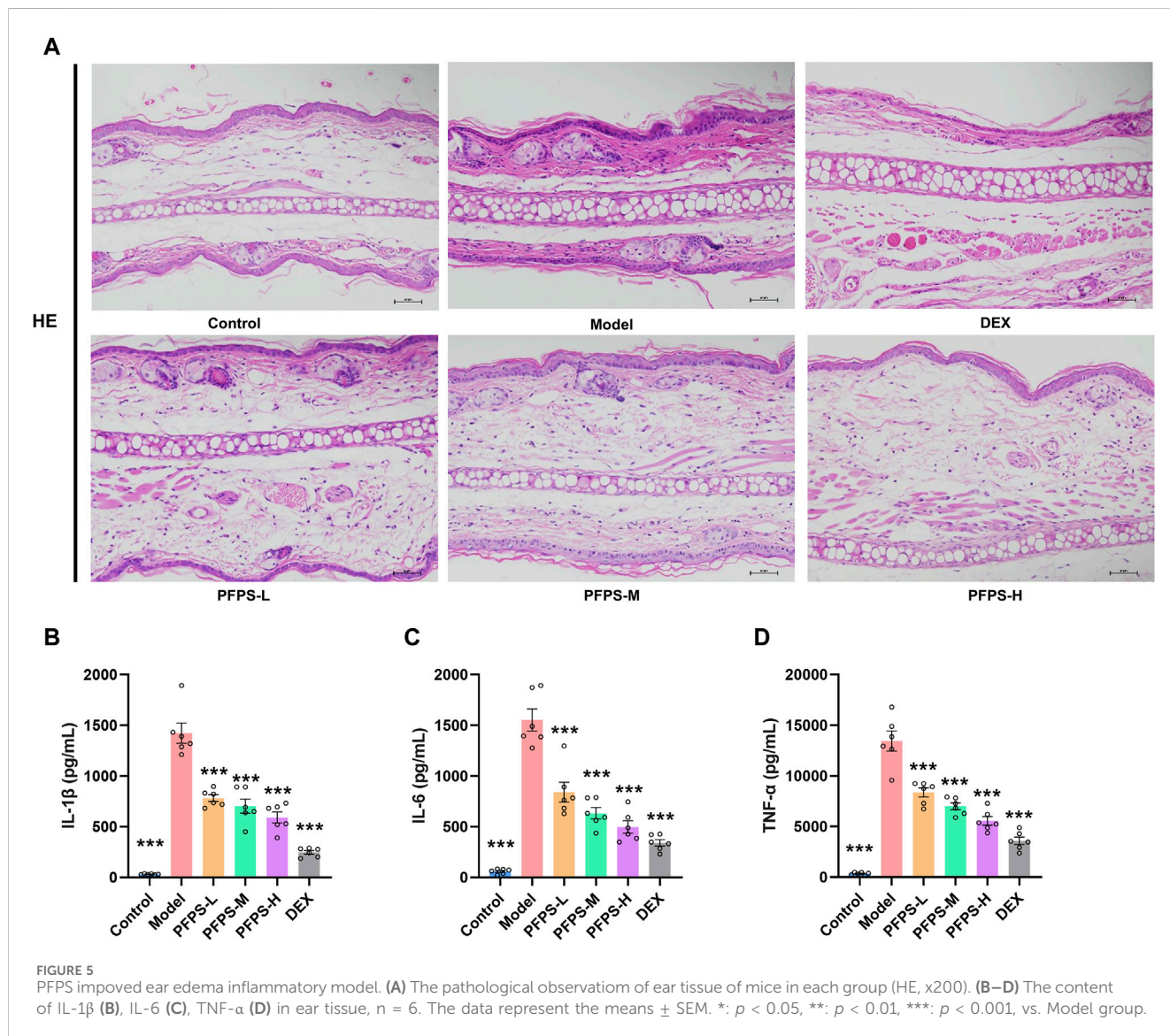
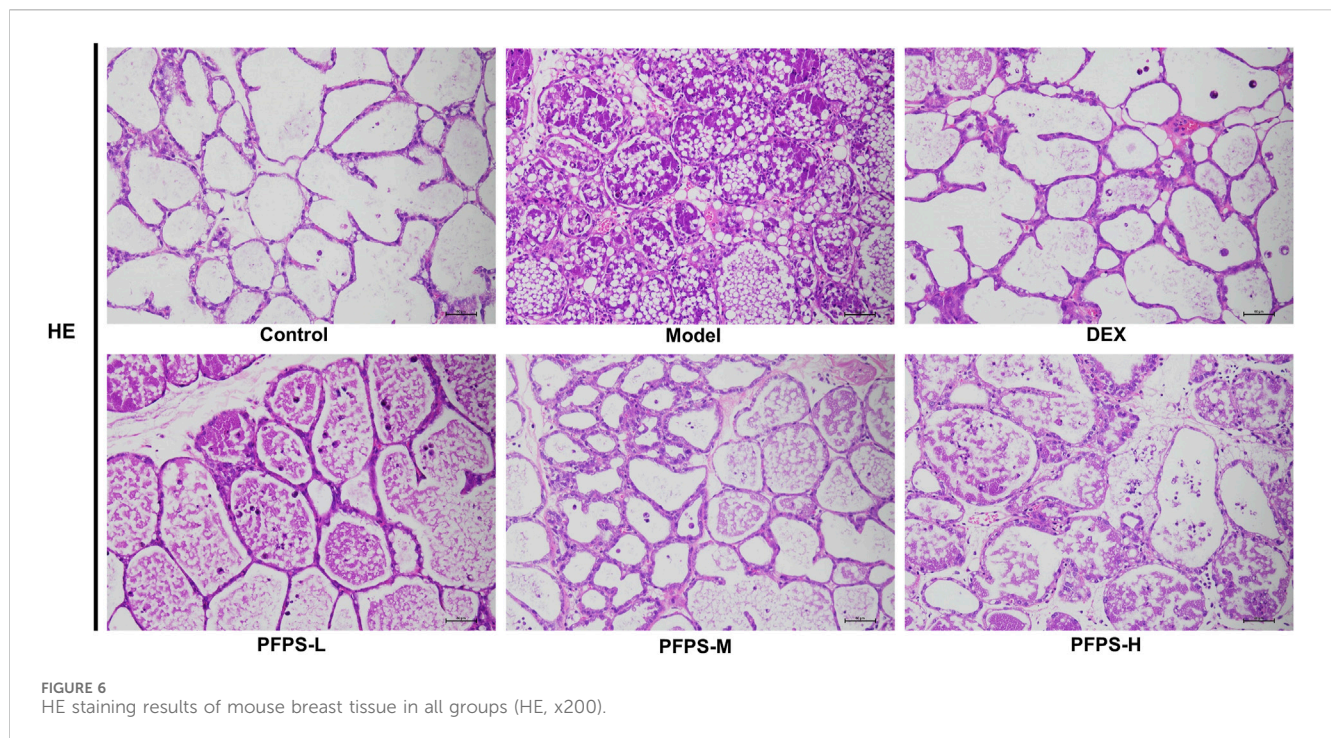


TABLE 6 Determination of mouse Paw Edema in each group.

Group	0 h	1 h	2 h	3 h	4 h	5 h	6 h
Model	1.05 ± 0.11	1.00 ± 0.31	1.36 ± 0.15	1.75 ± 0.22	1.37 ± 0.16	1.23 ± 0.13	1.67 ± 0.13
PFPS-L (400 mg/kg)	0.99 ± 0.21	0.74 ± 0.32	1.20 ± 0.17	1.32 ± 0.18	1.36 ± 0.15	1.16 ± 0.07	0.97 ± 0.18*
PFPS-M (800 mg/kg)	1.03 ± 0.27	0.96 ± 0.39	0.86 ± 0.12**	1.09 ± 0.19**	1.15 ± 0.26	0.96 ± 0.07*	0.84 ± 0.07*
PFPS-H (1600 mg/kg)	1.02 ± 0.12	1.09 ± 0.27	0.86 ± 0.22**	1.01 ± 0.13**	0.90 ± 0.20**	0.84 ± 0.12**	0.80 ± 0.21**
DEX (5 mg/kg)	0.98 ± 0.17	0.73 ± 0.26	0.77 ± 0.14**	0.90 ± 0.21**	0.67 ± 0.19**	0.64 ± 0.17**	0.59 ± 0.08***

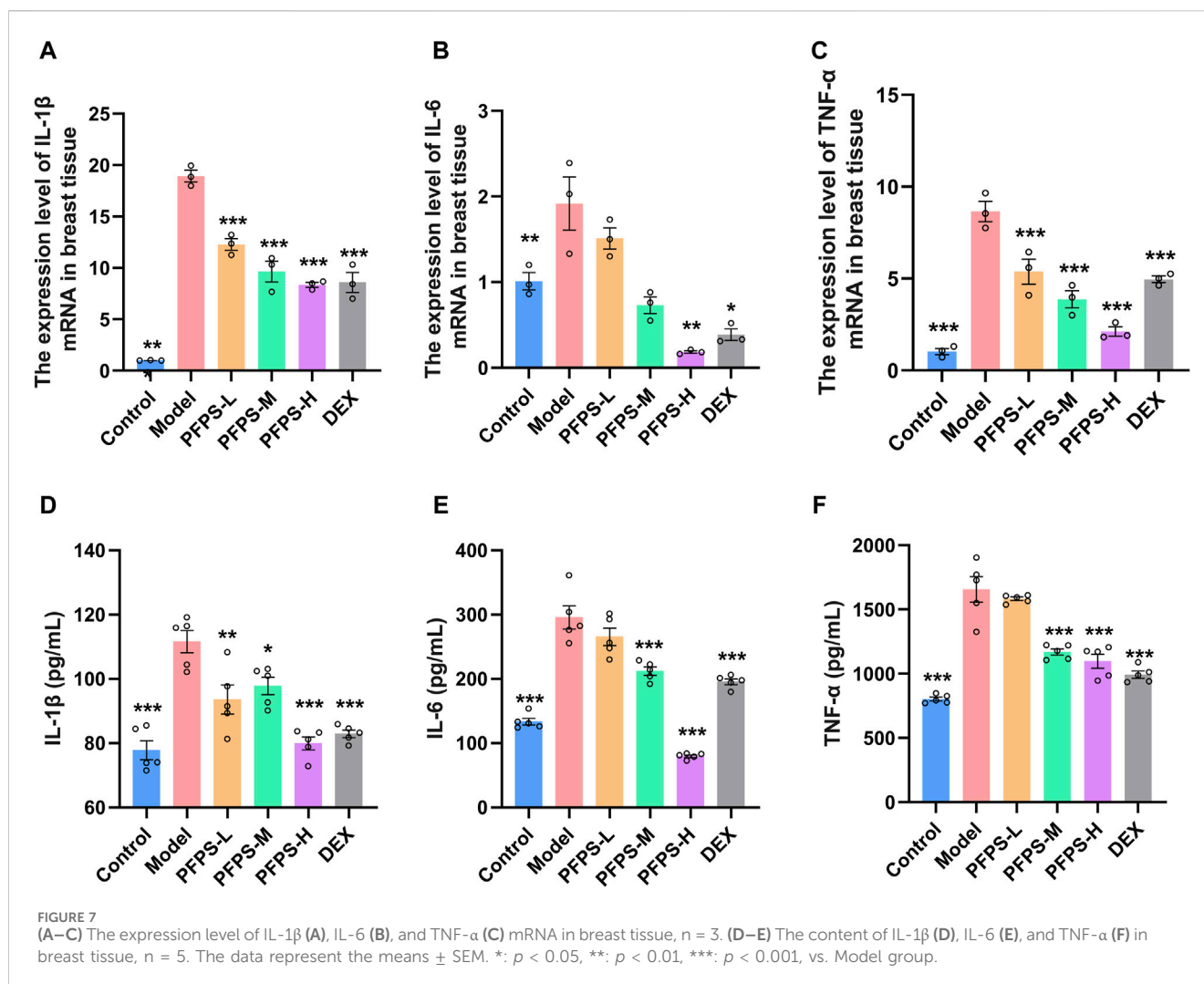
Note: The data represent the means ± SEM. *: $p < 0.05$, **: $p < 0.01$, ***: $p < 0.001$, vs. Model group.



increased inflammatory cells in the alveoli, and vascular congestion, which indicated that LPS modeling was successful. Compared with the Model group, the number of inflammatory cells in the DEX group was significantly reduced, with less inflammatory cell infiltration and mild congestion. There was inflammatory cell infiltration in all PFPS medication groups, among which PFPS-H had the best effect. To clarify the anti-inflammatory effect of PFPS, our experiment further detected the content of pro-inflammatory cytokines and the corresponding mRNA expression levels in mouse breast tissue. As shown in Figures 7A–F, PFPS significantly inhibited the mRNA expression levels of IL-1 β , IL-6, and TNF- α in the mammary tissue of model mice, and PFPS significantly reduced the contents of IL-1 β , IL-6, and TNF- α in breast tissue. Therefore, PFPS can significantly improve LPS-induced mammary gland inflammation in mice.

3.5 PFPS improved LPS-induced oxidative stress in mouse mammary gland tissue

LPS causes oxidative stress in inflammatory tissues, so oxidative stress-related indicators in mice breast tissue were detected. PFPS supplementation significantly improved the LPS-induced decrease in the levels of CAT, SOD, GSH, and T-AOC and the increase in MDA levels in breast tissue, and the PFPS high-dose group had the best effect (Figures 8A–E). PFPS also reduced MPO content in breast tissue (Figure 8F). PCR results showed that PFPS could significantly increase the mRNA expression of antioxidant-related enzymes in breast tissue (Figures 8G–I). Therefore, PFPS can significantly improve the oxidative stress in LPS-induced breast tissue in a dose-dependent manner.



3.6 PFPS effectively modulated intestinal flora in LPS-modeling mice

As shown in Figure 9A, supplementation with PFPS significantly increased the richness and diversity of the intestinal microbiota in mice. The PCOA plot based on the bray_curtis distance algorithm showed that the PFPS and Model groups were significantly separated (Figure 9B). Figure 9C shows the composition of the top 30 bacterial groups with relative abundance in each sample. Combined with the LDA discrimination chart shown in Figure 9D, the biomarkers under PFPS intervention were screened out, and their specific relative abundances are shown in Figure 9E. PFPS can suppress the relative abundance of *Odoribacter* and *AF12* and increase *Blautia*, *Parabacteroides*, *Allobaculum*, and *Clostridiaceae_Clostridium*. Therefore, PFPS can significantly modulate the composition of intestinal flora in mice.

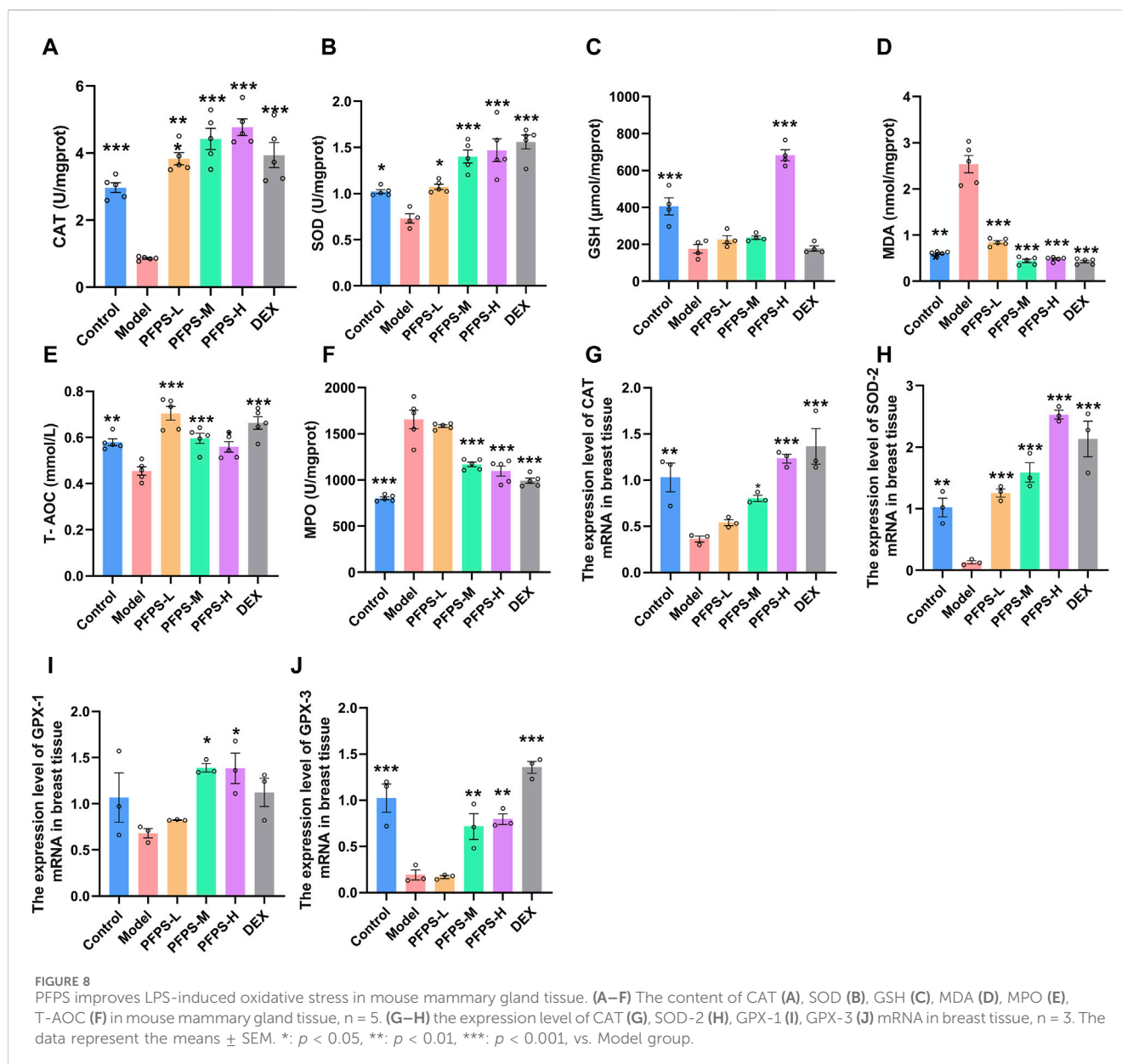
3.7 PFPS improves mastitis in mice by enhancing the blood-milk barrier

This experiment used immunofluorescence to measure the integrity of the blood-milk barrier. As shown in Figures 10–12,

LPS reduced the expression of barrier proteins Claudin-3 and Occludin, while the PFPS supplementation group and the DEX group antagonized the effects of LPS. Quantitative staining area results showed that PFPS could significantly increase the content of barrier proteins in LPS model mice, and the PFPS-H group had the best effect. PFPS-H caused high expression of Claudin-3 and Occludin, and their values were significantly higher than those in the blank and DEX groups. The expression levels of related genes were further tested and a consistent change trend was obtained. Therefore, PFPS can improve mouse mastitis by enhancing the blood-milk barrier.

4 Discussion

The PFPS was isolated and purified by ion-exchange column chromatography and gel column chromatography, and its chemical structure was characterized by using a combination of technique including infrared spectroscopy, liquid chromatography, gas chromatography, and NMR. The result revealed that the monosaccharides consist of GalA, Ara, and Gal, and the residues consist of 1,4-GalpA, 1,4-Galp, and 1,3,6-Galp, which may contain



HG-type and RG-I-type pectin structural domains. Similar methods have been validated for the identification of plant polysaccharides. For example, the chemical structure of licorice polysaccharide was identified and characterized by NMR and methylation analysis, and the result revealed that GPS-1 is composed of homogalacturonan (HG)-type pectin with 4)-D-GalpA-(1 as the backbone (Wu et al., 2022). Polysaccharide BAP1 of *Bifidobacterium adolescentis* CDM 368 consists of glucose, galactose, and rhamnose residues and was deduced by methylation analysis and NMR spectrum (Pacyga-Prus et al., 2023). The above results demonstrate the scientific validity of methylation and spectroscopy in elucidating the structure and composition of polysaccharides.

This experiment established an *in vitro* cell inflammation model by stimulating RAW264.7 cells with LPS. Macrophages are important immune cells involved in the initiation of inflammatory responses and play a key role in the pathogenesis of numerous inflammatory diseases by secreting large amounts of

pro-inflammatory mediators and pro-inflammatory cytokines (Wynn and Vannella, 2016; Oishi and Manabe, 2018). We found that PFPS can significantly inhibit the release of pro-inflammatory factors of RAW264.7 cells induced by LPS. Past research shows the release of pro-inflammatory factors increases significantly when inflammation occurs (Huang et al., 2023). LPS can promote the secretion of cytokines TNF- α , IL-6, and IL-1 β (Wang et al., 2020). As intercellular signaling molecules, these factors can attract neutrophils in the blood into the infected area to eliminate pathogens, but they can also cause damage to breast tissue, resulting in cell necrosis and suppuration (O'Neill et al., 2016). Experiment results showed that PFPS also significantly inhibited the phagocytosis of neutral red dye and *E. coli* by RAW264.7 cells. Macrophages present antigens through phagocytosis, and LPS can induce the enhancement of phagocytosis of RAW264.7 cells by regulating the JNK signaling pathway and promoting the occurrence of inflammation (Yuan et al., 2019; Chen et al., 2021). In summary,

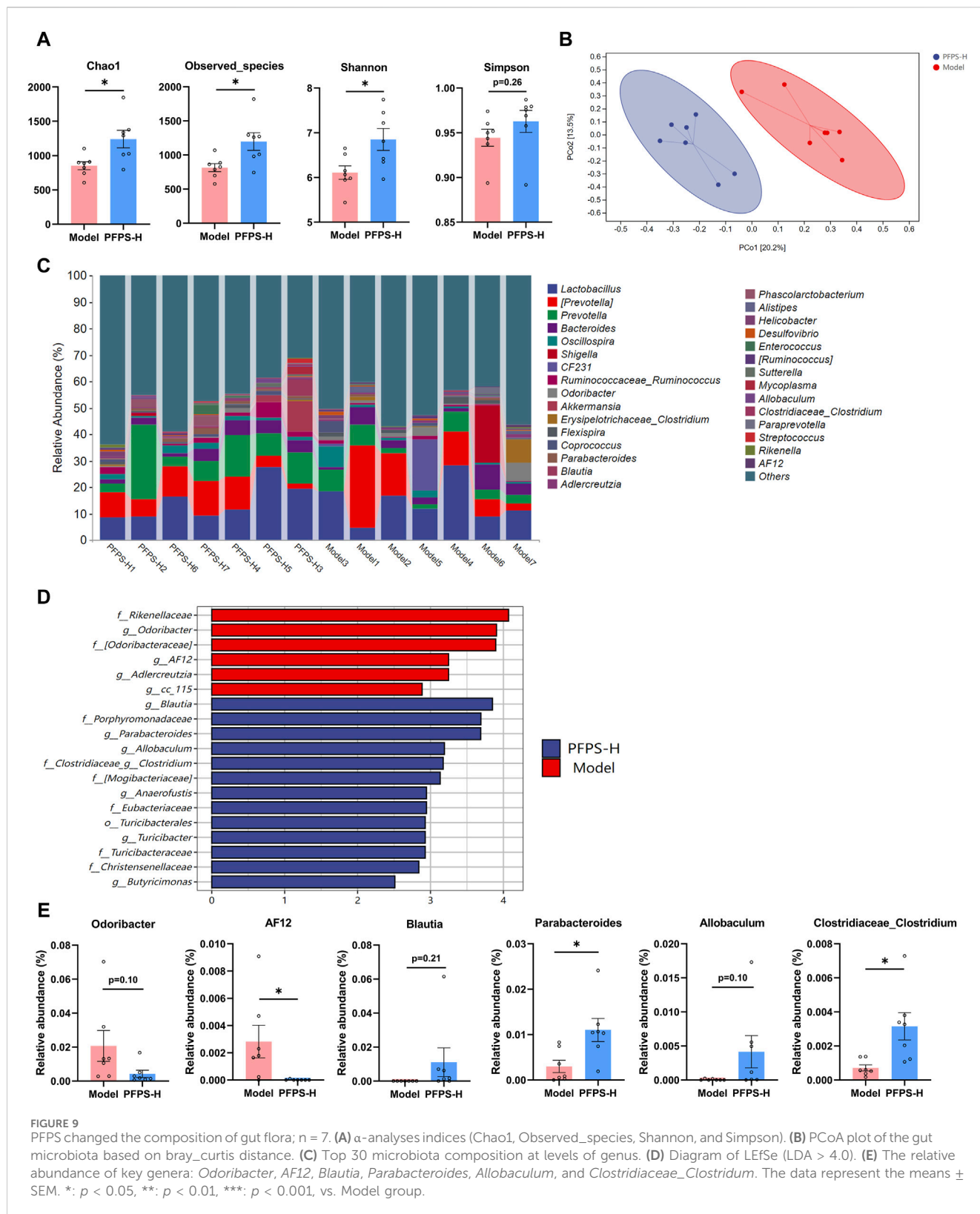


FIGURE 9 PFPS changed the composition of gut flora; n = 7. (A) α -analyses indices (Chao1, Observed_species, Shannon, and Simpson). (B) PCoA plot of the gut microbiota based on bray_curtis distance. (C) Top 30 microbiota composition at levels of genus. (D) Diagram of LefSe (LDA > 4.0). (E) The relative abundance of key genera: *Odoribacter*, *AF12*, *Blautia*, *Parabacteroides*, *Allobaculum*, and *Clostridiaceae_Clostridium*. The data represent the means \pm SEM. *: $p < 0.05$, **: $p < 0.01$, ***: $p < 0.001$, vs. Model group.

PFPS exhibits significant inflammation-inhibitory effects *in vitro* models.

This experiment preliminarily evaluated the *in vitro* inflammation inhibitory effect of PFPS through mouse ear swelling and foot swelling models. The ear swelling model is

widely used in evaluation experiments of anti-inflammatory drugs, in which xylene induces the ear swelling model by activating phospholipase A2 (Santos et al., 2012). The pathological process of ear swelling is closely related to the increase in pro-inflammatory factors, such as IL-1 β is considered

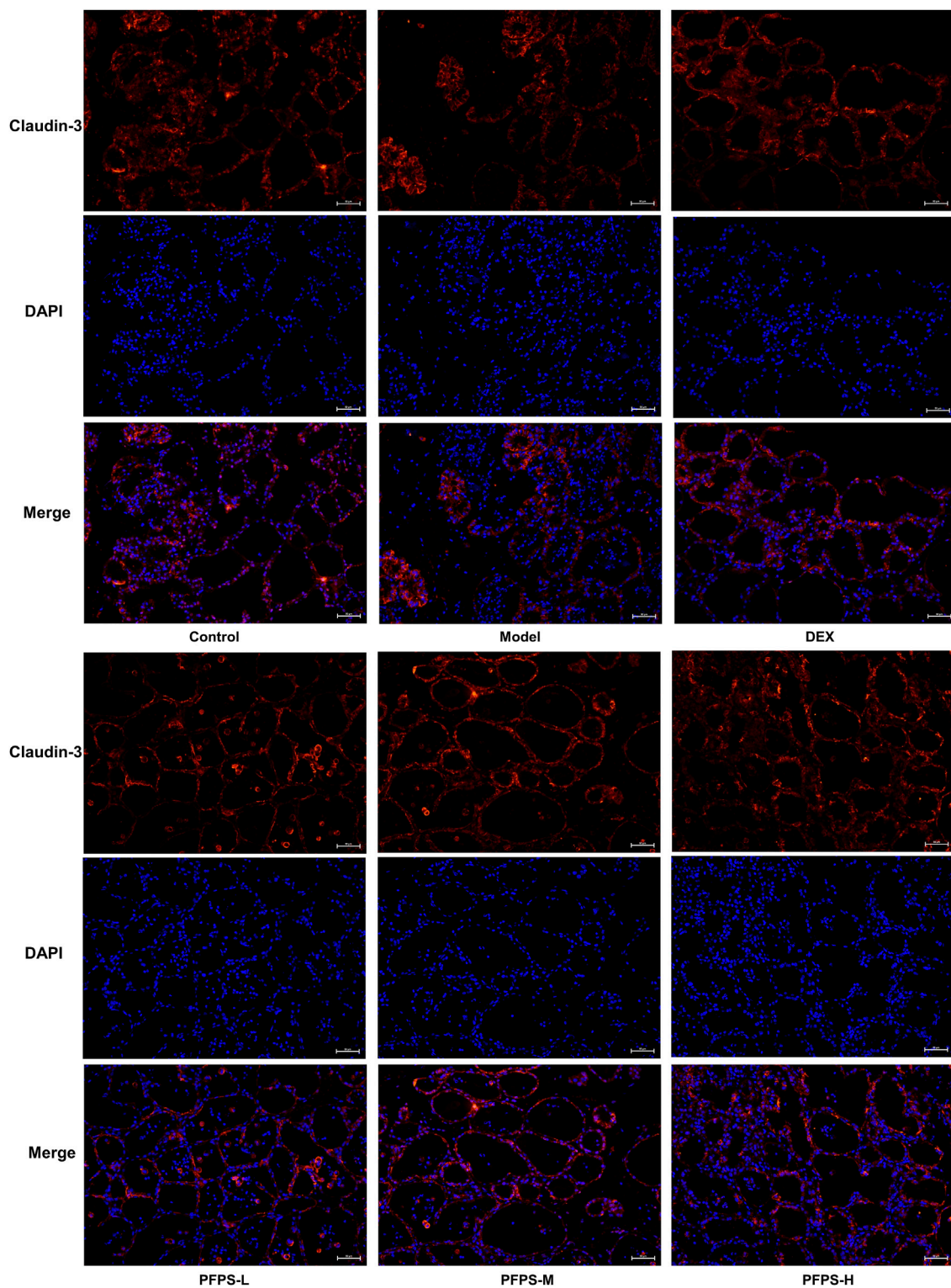


FIGURE 10 Immunofluorescence staining of Claudin-3 in breast tissue (x200).

to be the main cytokine in the initiation of acute inflammation mediated by keratinocytes (Soromou et al., 2012). The paw swelling model in mice is also a widely recognized model of inflammation *in vivo* (Zhang et al., 2022; Hijazy et al., 2023). The results showed that PFPS significantly inhibited ear swelling and

foot swelling, showing a significant inhibitory effect on inflammation *in vivo*.

PFPS had shown anti-inflammatory effects in both *in vivo* and *in vitro* models, so we further evaluated the anti-inflammatory effects and potential intervention pathways of PFPS in a mouse

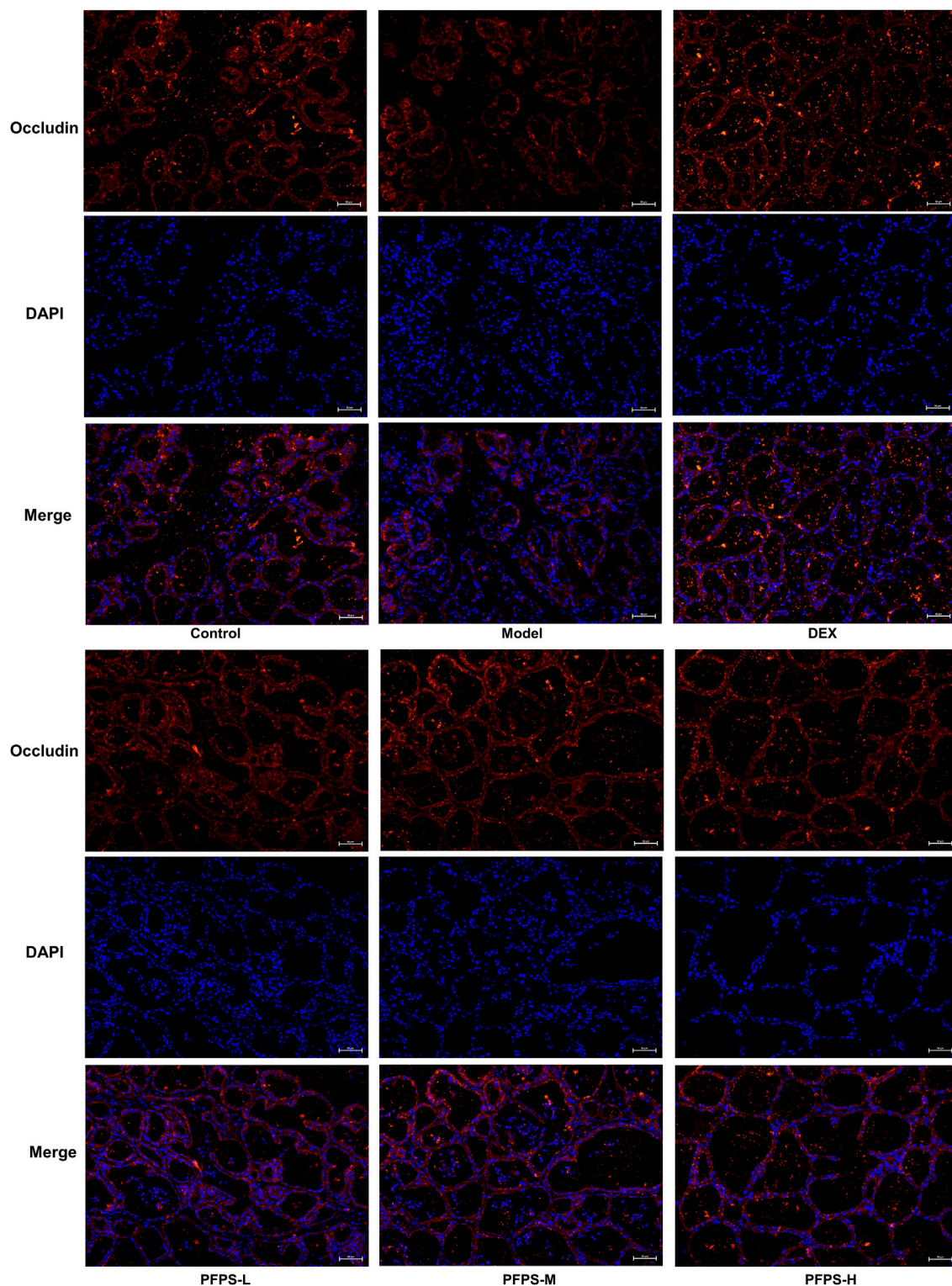
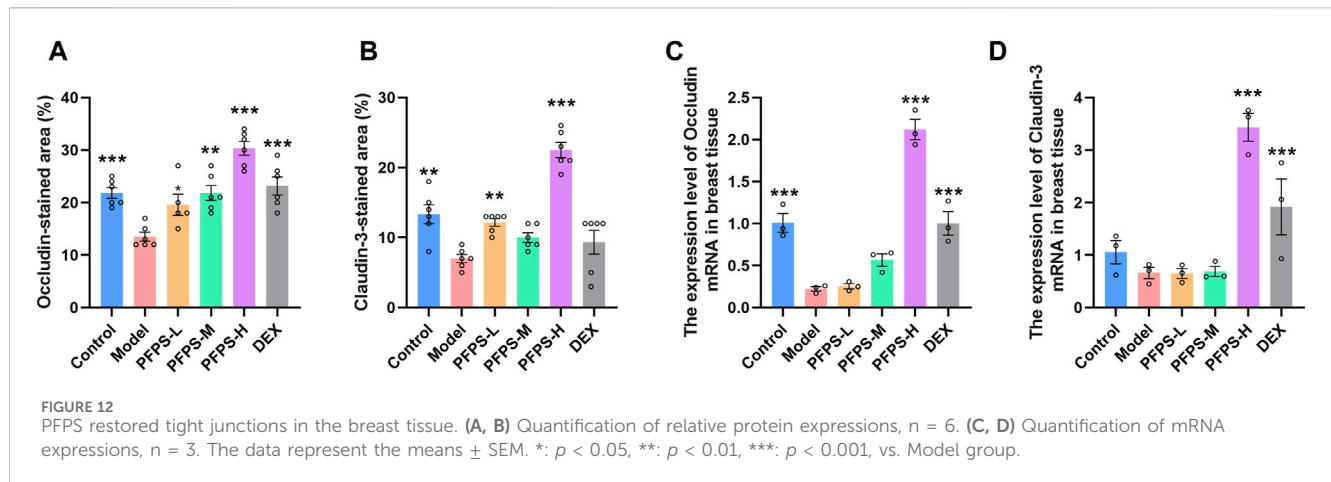


FIGURE 11
Immunofluorescence staining of Occludin in breast tissue (x200).

mastitis model. LPS can induce oxidative stress in breast tissue (increased intracellular ROS, MDA, and decreased SOD, GSH-Px and CAT activity), and oxidative stress aggravates tissue inflammation by increasing the release of inflammatory factors (increased expression of IL-6, IL-1 β , and TNF- α) (Ali et al.,

2022). The results showed that high-dose PFPS significantly improved the oxidative stress in the mammary gland of model mice and antagonized the increase in the contents and mRNA expression levels of IL-1 β , IL-6, and TNF- α . Research on polysaccharides shows that most polysaccharides exert systemic



effects by regulating intestinal flora (Tang et al., 2019; Liu et al., 2023). At the same time, considering that PFPS has a significant inhibitory effect on inflammation in models of mastitis, ear swelling, and paw swelling, we believe that PFPS may regulate systemic inflammation by regulating intestinal flora. Sequencing results showed that PFPS significantly changed the composition of intestinal flora in model mice. PFPS decreased the relative abundance of *Oscillospira* and *AF12*. *Oscillospira* is a common opportunistic pathogen closely associated with inflammation (Xu R. et al., 2022). Zhu et al., (2020) found that *Oscillospira* positively correlates with diabetes and inflammation while feeding mice oat-resistant-starch can significantly inhibit *Oscillospira* and improve inflammation. Wei et al., (2023) found that Glycyrrhiza polysaccharide can inhibit *Oscillospira* and improve DSS-induced intestinal inflammation. PFPS also reduced the relative abundance of *Odoribacter*. Andrea et al. found that *Odoribacter* was positively correlated with the degree of inflammation in the body and that *Odoribacter* could cause systemic inflammation when studying neuroinflammation and intestinal flora (Quagliariello et al., 2018). PFPS increased the relative abundance of *Blautia*, *Parabacteroides*, *Allobaculum*, and *Clostridium*. *Blautia* is a butyrate producer and regulates the metabolic processes of animals through exogenous butyrate supplementation (Zhou et al., 2017). Related studies have shown that butyrate supplementation can alleviate LPS damage to the blood-milk barrier and reduce inflammatory responses (Wang et al., 2017a). *Parabacteroides* and *Allobaculum* are the common probiotic that has anti-inflammatory effects and produces SCFA (Cui et al., 2022; Zhang et al., 2023). Wu et al. (2019) found that supplied *Hirsutella sinensis* polysaccharide can increase the relative abundance of *Parabacteroides goldsteinii*. Supplementation of *P. goldsteinii* alone can significantly reduce the content of inflammatory factors in serum, and improve inflammation and intestinal barrier. *Allobaculum* can increase the levels of intestinal and blood-brain barrier proteins, attenuate the effects of LPS and alleviate neuroinflammation (Yuan et al., 2022). *Clostridium* also has anti-inflammatory effects. Related studies have shown that *Clostridium leptum* can induce the production of IL-10⁺ regulatory B cells to treat airway inflammation (Huang et al., 2022). Studies have shown that intestinal SCFA-producing bacteria can protect the blood-milk barrier and improve mastitis

through SCFA (Hu et al., 2020). Ran et al. demonstrated that hesperidin significantly improved the blood-milk barrier by increasing acetic acid and propionic acid producing bacteria (Ran et al., 2024). Hu et al. found that supplementation with butyrate-producing bacteria significantly reduced the permeability of the blood-milk barrier and inhibited the occurrence of mastitis (Hu et al., 2020). Our results showed that PFPS significantly restored LPS-induced BMB disruption by promoting the content and mRNA expression of tight junction proteins Claudin-3 and Occludin. Therefore, PFPS exerts anti-mastitis effects by increasing the relative abundance of SCFA-producing bacteria and improving the blood-milk barrier.

5 Conclusion

PFPS reduced the production of proinflammatory factors and inhibited the phagocytic ability of RAW264.7 cells *in vitro*. PFPS showed significant anti-inflammatory effects *in vivo* model of mouse ear swelling, foot swelling, and mastitis. 16S RNA sequencing results showed that PFPS significantly regulated the composition of mouse intestinal flora, decreased the relative abundance of *Oscillospira* and *AF12*, and increased *Blautia*, *Parabacteroides*, *Allobaculum*, and *Clostridium*. Therefore, PFPS reduced LPS-induced mastitis by regulating intestinal flora and improving the blood-milk barrier. There are still many deficiencies in this article, for example: the effect of PFPS on regulating intestinal flora requires FMT experiments for inflammation; at the same time, due to the limitations of sequencing technology, the specific flora regulated by PFPS cannot be accurately determined; whether the regulatory effect of PFPS *in vitro* experiments can occur *in vivo* independently of regulating flora still needs to be verified by germ-free mice.

Data availability statement

The datasets presented in this study can be found in online repositories. The names of the repository/repositories and accession number(s) can be found in the article/supplementary material.

Ethics statement

The animal study was approved by Animal Ethics Committee of Xinjiang Agricultural University. The study was conducted in accordance with the local legislation and institutional requirements.

Author contributions

JL: Conceptualization, Data curation, Investigation, Methodology, Validation, Visualization, Writing—original draft. WY: Writing—review and editing. YL: Writing—review and editing. ZY: Writing—review and editing. LL: Data curation, Writing—original draft. ZM: Writing—review and editing. XY: Writing—review and editing. YL: Writing—review and editing. ZZ: Writing—review and editing. SA: Writing—review and editing. YW: Writing—review and editing, Investigation. AW: Writing—review and editing. QG: Writing—review and editing, Writing—original draft.

Funding

The author(s) declare that financial support was received for the research, authorship, and/or publication of this article. The study was supported by Integration and Demonstrations of Donkey

References

- Ali, I., Li, C., Kuang, M., Shah, A. U., Shafiq, M., Ahmad, M. A., et al. (2022). Nrf2 Activation and NF-Kb and caspase/bax signaling inhibition by sodium butyrate alleviates LPS-induced cell injury in bovine mammary epithelial cells. *Mol. Immunol.* 148, 54–67. doi:10.1016/j.molimm.2022.05.121
- Aoki, R., Onuki, M., Hattori, K., Ito, M., Yamada, T., Kamikado, K., et al. (2021). Commensal microbe-derived acetate suppresses NAFLD/NASH development via hepatic FFAR2 signalling in mice. *Microbiome* 9 (1), 188. doi:10.1186/s40168-021-01125-7
- Caruso, A., Barbarossa, A., Tassone, A., Ceramella, J., Carocci, A., Catalano, A., et al. (2020). Pomegranate: nutraceutical with promising benefits on human health. *Appl. Sci.* 10, 6915. doi:10.3390/app10196915
- Chen, M., Tung, Y., Hu, C., Chang, H., Lin, W., and Sheu, S. (2021). Three lipid emulsions reduce Staphylococcus aureus-stimulated phagocytosis in mouse RAW264.7 cells. *Microorganisms* 9 (12), 2479. doi:10.3390/microorganisms9122479
- Colombo, E., Sangiovanni, E., Dell'Agli, M., and Heber, D. (2013). A review on the anti-inflammatory activity of pomegranate in the gastrointestinal tract. *Evid.-based Complement. Altern. Med.* 2013, 247145. doi:10.1155/2013/247145
- Cui, Y., Zhang, L., Wang, X., Yi, Y., Shan, Y., Liu, B., et al. (2022). Roles of intestinal Parabacteroides in human health and diseases. *FEMS Microbiol. Lett.* 369 (1), fnac072. doi:10.1093/femsle/fnac072
- Faria, A., and Calhau, C. (2011). The bioactivity of pomegranate: impact on health and disease. *Crit. Rev. Food. Sci. Nutr.* 51 (7), 626–634. doi:10.1080/10408391003748100
- George, N., Abukhader, M., Al Balushi, K., Al Sabahi, B., and Khan, S. A. (2023). An insight into the neuroprotective effects and molecular targets of pomegranate (Punica granatum) against Alzheimer's disease. *Nutr. Neurosci.* 26 (10), 975–996. doi:10.1080/1028415X.2022.2121092
- Gillespie, B. E., and Oliver, S. P. (2005). Simultaneous detection of mastitis pathogens, *Staphylococcus aureus*, *Streptococcus uberis*, and *Streptococcus agalactiae* by multiplex real-time polymerase chain reaction. *J. Dairy. Sci.* 88 (10), 3510–3518. doi:10.3168/jds.S0022-0302(05)73036-8
- Guidry, A. J., O'Brien, C. N., and Douglass, L. W. (1998). A bovine mammary endothelial/epithelial cell culture model of the blood/milk barrier. *Can. J. veterinary Res.* 62 (2), 117–121.
- Hijazy, H. H. A., Dahran, N., Althagafi, H. A., Alharthi, F., Habotta, O. A., Oyouni, A. A., et al. (2023). Thymoquinone counteracts oxidative and inflammatory machinery in carrageenan-induced murine paw edema model. *Environ. Sci. Pollut. Res.* 30 (6), 16597–16611. doi:10.1007/s11356-022-23343-8
- Industry in Southern Xinjiang (No. 2020B01002-2-3), National Key Research and Development Program of China (No. 2021YFD1600702-3) and National Natural Science Foundation of China (NSFC, Grant No. 32202855 and 32172900).
- Hosseini, A., Razavi, B. M., and Hosseinzadeh, H. (2023). Protective effects of pomegranate (*Punica granatum*) and its main components against natural and chemical toxic agents: a comprehensive review. *Phytomedicine* 109, 154581. doi:10.1016/j.phymed.2022.154581
- Hu, X., Guo, J., Zhao, C., Jiang, P., Maimai, T., Yanyi, L., et al. (2020). The gut microbiota contributes to the development of Staphylococcus aureus-induced mastitis in mice. *ISME J.* 14 (7), 1897–1910. doi:10.1038/s41396-020-0651-1
- Hu, X., Li, S., Fu, Y., and Zhang, N. (2019). Targeting gut microbiota as a possible therapy for mastitis. *Eur. J. Clin. Microbiol. Infect. Dis.* 38 (8), 1409–1423. doi:10.1007/s10096-019-03549-4
- Huang, F., Zhang, Y., Bai, X., Wang, C., and Li, Y. (2022). Clostridium leptum induces the generation of interleukin-10+ regulatory B cells to alleviate airway inflammation in asthma. *Mol. Immunol.* 145, 124–138. doi:10.1016/j.molimm.2022.03.010
- Huang, Y., Ye, Y., Xu, D., Ji, J., Sun, J., Xu, M., et al. (2023). Structural characterization and anti-inflammatory activity of a novel neutral polysaccharide isolated from *Smilax glabra* Roxb. *Int. J. Biol. Macromol.* 234, 123559. doi:10.1016/j.ijbiomac.2023.123559
- Karimi, M., Sadeghi, R., and Kokini, J. (2017). Pomegranate as a promising opportunity in medicine and nanotechnology. *Trends Food Sci. Technol.* 69, 59–73. doi:10.1016/j.tifs.2017.08.019
- Lansky, E. P., and Newman, R. A. (2007). *Punica granatum* (pomegranate) and its potential for prevention and treatment of inflammation and cancer. *J. Ethnopharmacol.* 109 (2), 177–206. doi:10.1016/j.jep.2006.09.006
- Leesombun, A., Sariya, L., Taowan, J., Nakthong, C., Thongjuy, O., and Boonmasawai, S. (2022). Natural antioxidant, antibacterial, and antiproliferative activities of ethanolic extracts from *Punica granatum* L. Tree barks mediated by extracellular signal-regulated kinase. *Plants* 11, 2258. doi:10.3390/plants11172258
- Li, K., Ran, X., Zeng, Y., Li, S., Hu, G., Wang, X., et al. (2023). Maslinic acid alleviates LPS-induced mice mastitis by inhibiting inflammatory response, maintaining the integrity of the blood-milk barrier and regulating intestinal flora. *Int. Immunopharmacol.* 122, 110551. doi:10.1016/j.intimp.2023.110551
- Li, Y., Qi, Y., Huang, T. H. W., Yamahara, J., and Roufogalis, B. D. (2008). Pomegranate flower: a unique traditional antidiabetic medicine with dual PPAR- α - γ activator properties. *Diabetes, Obes. Metabolism* 10 (1), 10–17. doi:10.1111/j.1463-1326.2007.00708.x
- Liu, J., Chen, B., Jiang, M., Cui, T., Lv, B., Fu, Z., et al. (2023). Polygonatum odoratum polysaccharide attenuates lipopolysaccharide-induced lung injury in mice by regulating gut microbiota. *Food Sci. Nutr.* 11, 6974–6986. doi:10.1002/fsn3.3622

Conflict of interest

The authors declare that the research was conducted in the absence of any commercial or financial relationships that could be construed as a potential conflict of interest.

The author(s) declared that they were an editorial board member of Frontiers, at the time of submission. This had no impact on the peer review process and the final decision.

Publisher's note

All claims expressed in this article are solely those of the authors and do not necessarily represent those of their affiliated organizations, or those of the publisher, the editors and the reviewers. Any product that may be evaluated in this article, or claim that may be made by its manufacturer, is not guaranteed or endorsed by the publisher.

- Liu, Y., and Seeram, N. P. (2018). Liquid chromatography coupled with time-of-flight tandem mass spectrometry for comprehensive phenolic characterization of pomegranate fruit and flower extracts used as ingredients in botanical dietary supplements. *J. Sep. Sci.* 41 (15), 3022–3033. doi:10.1002/jssc.201800480
- Middha, S. K., Usha, T., and Pande, V. (2013). A review on antihyperglycemic and antihepatoprotective activity of eco-friendly Punica granatum peel waste. *Evid.-based Complement. Altern. Med.* 2013, 656172. doi:10.1155/2013/656172
- Oishi, Y., and Manabe, I. (2018). Macrophages in inflammation, repair and regeneration. *Int. Immunol.* 30 (11), 511–528. doi:10.1093/intimm/dxy054
- O'Neill, L. A., Kishon, R. J., and Rathmell, J. (2016). A guide to immunometabolism for immunologists. *Nat. Rev. Immunol.* 16 (9), 553–565. doi:10.1038/nri.2016.70
- Pacyga-Prus, K., Jakubczyk, D., Sandstrom, C., Srutkova, D., Pyclik, M. J., Leszczynska, K., et al. (2023). Polysaccharide BAP1 of *Bifidobacterium adolescentis* CDDM 368 is a biologically active molecule with immunomodulatory properties. *Carbohydr. Polym.* 315, 120980. doi:10.1016/j.carbpol.2023.120980
- Quagliarriello, A., Del, C. F., Russo, A., Reddel, S., Conte, G., Lopetuso, L. R., et al. (2018). Gut microbiota profiling and gut-brain crosstalk in children affected by pediatric acute-onset neuropsychiatric syndrome and pediatric autoimmune neuropsychiatric disorders associated with streptococcal infections. *Front. Microbiol.* 9, 675. doi:10.3389/fmicb.2018.00675
- Ran, X., Hu, G., Guo, W., Li, K., Wang, X., Liu, J., et al. (2024). Hesperetin regulates the intestinal flora and inhibits the TLR4/NF- κ B signaling axis to protect the blood-milk barrier and prevent mastitis. *Life Sci.* 342, 122533. doi:10.1016/j.lfs.2024.122533
- Santos, J. A., Arruda, A., Silva, M. A., Cardoso, C. A., Vieira, M. C., Kassuya, C. A., et al. (2012). Anti-inflammatory effects and acute toxicity of hydroethanolic extract of *Jacaranda decurrens* roots in adult male rats. *J. Ethnopharmacol.* 144 (3), 802–805. doi:10.1016/j.jep.2012.10.024
- Soromou, L. W., Chen, N., Jiang, L., Huo, M., Wei, M., Chu, X., et al. (2012). Astragaloside attenuates lipopolysaccharide-induced inflammatory responses by down-regulating NF- κ B signaling pathway. *Biochem. Biophys. Res. Commun.* 419 (2), 256–261. doi:10.1016/j.bbrc.2012.02.005
- Sun, W., Wu, E., Zhang, G., Xu, B., Chen, X., Hao, K., et al. (2022). Total flavonoids of *Abrus cantoniensis* inhibit CD14/TLR4/NF- κ B/MAPK pathway expression and improve gut microbiota disorders to reduce lipopolysaccharide-induced mastitis in mice. *Front. Microbiol.* 13. doi:10.3389/fmicb.2022.985529
- Tang, C., Ding, R., Sun, J., Liu, J., Kan, J., and Jin, C. (2019). The impacts of natural polysaccharides on intestinal microbiota and immune responses - a review. *Food Funct.* 10 (5), 2290–2312. doi:10.1039/c8fo01946k
- Tsugami, Y., Matsunaga, K., Suzuki, T., Nishimura, T., and Kobayashi, K. (2017). Phytoestrogens weaken the blood–milk barrier in lactating mammary epithelial cells by affecting tight junctions and cell viability. *J. Agric. Food. Chem.* 65 (50), 11118–11124. doi:10.1021/acs.jafc.7b04786
- Vucic, V., Grabez, M., Trchounian, A., and Arsic, A. (2019). Composition and potential health benefits of pomegranate: a review. *Curr. Pharm. Des.* 25 (16), 1817–1827. doi:10.2174/1381612825666190708183941
- Wang, D., Ozen, C., Abu-Reidah, I. M., Chigurupati, S., Patra, J. K., Horbanczuk, J. O., et al. (2018). Vasculoprotective effects of pomegranate (*Punica granatum* L.). *Front. Pharmacol.* 9, 544. doi:10.3389/fphar.2018.00544
- Wang, J., Wei, Z., Zhang, X., Wang, Y., Fu, Y., and Yang, Z. (2017a). Butyrate protects against disruption of the blood-milk barrier and moderates inflammatory responses in a model of mastitis induced by lipopolysaccharide. *Br. J. Pharmacol.* 174 (21), 3811–3822. doi:10.1111/bph.13976
- Wang, J., Wei, Z., Zhang, X., Wang, Y., Yang, Z., and Fu, Y. (2017b). Propionate protects against lipopolysaccharide-induced mastitis in mice by restoring blood–milk barrier disruption and suppressing inflammatory response. *Front. Immunol.* 8, 1108. doi:10.3389/fimmu.2017.01108
- Wang, Y., Teng, G., Zhou, H., and Dong, C. (2020). Germanium reduces inflammatory damage in mammary glands during lipopolysaccharide-induced mastitis in mice. *Biol. Trace Elem. Res.* 198 (2), 617–626. doi:10.1007/s12011-020-02106-x
- Wei, X., Li, N., Wu, X., Cao, G., Qiao, H., Wang, J., et al. (2023). The preventive effect of Glycyrrhiza polysaccharide on lipopolysaccharide-induced acute colitis in mice by modulating gut microbial communities. *Int. J. Biol. Macromol.* 239, 124199. doi:10.1016/j.ijbiomac.2023.124199
- Wei, Y., Khalaf, A. T., Ye, P., Fan, W., Su, J., Chen, W., et al. (2022). Therapeutic benefits of pomegranate flower extract: a novel effect that reduces oxidative stress and significantly improves diastolic relaxation in hyperglycemic *in vitro* in rats. *Altern. Med.* 2022, 4158762. doi:10.1155/2022/4158762
- Wibaut, J. P., and Hollstein, U. (1957). Investigation of the alkaloids of *Punica granatum* L. *Arch. Biochem. Biophys.* 69, 27–32. doi:10.1016/0003-9861(57)90468-X
- Wu, T. R., Lin, C. -S., Chang, C. -J., Lin, T. -L., Martel, J., Ko, Y. -F., et al. (2019). Gut commensal *Parabacteroides goldsteinii* plays a predominant role in the anti-obesity effects of polysaccharides isolated from *Hirsutiella sinensis*. *Gut* 68 (2), 248–262. doi:10.1136/gutjnl-2017-315458
- Wu, Y., Zhou, H., Wei, K., Zhang, T., Che, Y., Nguyen, A. D., et al. (2022). Structure of a new glycyrrhiza polysaccharide and its immunomodulatory activity. *Front. Immunol.* 13, 1007186. doi:10.3389/fimmu.2022.1007186
- Wynn, T. A., and Vannella, K. M. (2016). Macrophages in tissue repair, regeneration, and fibrosis. *Immunity* 44 (3), 450–462. doi:10.1016/j.immuni.2016.02.015
- Xu, D., Zhuang, L., Gao, S., Ma, H., Cheng, J., Liu, J., et al. (2022a). Orally administered ginkgolide C attenuates DSS-induced colitis by maintaining gut barrier integrity, inhibiting inflammatory responses, and regulating intestinal flora. *J. Agric. Food. Chem.* 70 (46), 14718–14731. doi:10.1021/acs.jafc.2c06177
- Xu, R., Zhu, M., Cao, J., and Guo, M. (2022b). Tea polyphenols protect the mammary gland of dairy cows by enhancing antioxidant capacity and regulating the TGF- β 1/p38/JNK pathway. *Metabolites* 12, 1009. doi:10.3390/metabo12111009
- Yang, Y., Lv, L., Shi, S., Cai, G., Yu, L., Xu, S., et al. (2023). Polysaccharide from walnut green husk alleviates liver inflammation and gluconeogenesis dysfunction by altering gut microbiota in ochratoxin A-induced mice. *Carbohydr. Polym.* 322, 121362. doi:10.1016/j.carbpol.2023.121362
- Yuan, L., Zhang, F., Shen, M., Jia, S., and Xie, J. (2019). Phytosterols suppress phagocytosis and inhibit inflammatory mediators via ERK pathway on LPS-triggered inflammatory responses in RAW264.7 macrophages and the correlation with their structure. *Foods* 8 (11), 582. doi:10.3390/foods8110582
- Yuan, S., Yang, J., Jian, Y., Lei, Y., Yao, S., Hu, Z., et al. (2022). Treadmill exercise modulates intestinal microbes and suppresses LPS displacement to alleviate neuroinflammation in the brains of APP/PS1 mice. *Nutrients* 14 (19), 4134. doi:10.3390/nu14194134
- Yue, F., Zhang, J., Xu, J., Niu, T., Lu, X., and Liu, M. (2022). Effects of monosaccharide composition on quantitative analysis of total sugar content by phenol-sulfuric acid method. *Front. Nutr.* 9, 963318. doi:10.3389/fnut.2022.963318
- Zhang, L., Zhang, T., Sun, J., Huang, Y., Liu, T., Ye, Z., et al. (2023). Calorie restriction ameliorates hyperglycemia, modulates the disordered gut microbiota, and mitigates metabolic endotoxemia and inflammation in type 2 diabetic rats. *J. Endocrinol. Invest.* 46 (4), 699–711. doi:10.1007/s40618-022-01914-3
- Zhang, X., Retyunskiy, V., Qiao, S., Zhao, Y., and Tzeng, C. (2022). Alloferon-1 ameliorates acute inflammatory responses in λ -carrageenan-induced paw edema in mice. *Sci. Rep.* 12 (1), 16689. doi:10.1038/s41598-022-20648-z
- Zhou, D. A., Pan, Q., Xin, F., Zhang, R., He, C., Chen, G., et al. (2017). Sodium butyrate attenuates high-fat diet-induced steatohepatitis in mice by improving gut microbiota and gastrointestinal barrier. *World J. Gastroenterol.* 23 (1), 60–75. doi:10.3748/wjg.v23.i1.60
- Zhu, Y., Dong, L., Huang, L., Shi, Z., Dong, J., Yao, Y., et al. (2020). Effects of oat β -glucan, oat resistant starch, and the whole oat flour on insulin resistance, inflammation, and gut microbiota in high-fat-diet-induced type 2 diabetic rats. *J. Funct. Foods.* 69, 103939. doi:10.1016/j.jff.2020.103939